AD-A073 540 SCIENCE APPLICATIONS INC MCLEAN VA OCEAN SCIENCE DIV F/G 4/2
A MODEL OF DIURNAL VARIABILITY OF THE OCEAN-ATMOSPHERE SYSTEM I--ETC(U)
JUL 79 R M CLANCY N00014-78-C-0287
UNCLASSIFIED SAI-79-807-WA NL

1 OF 2
AD A073540

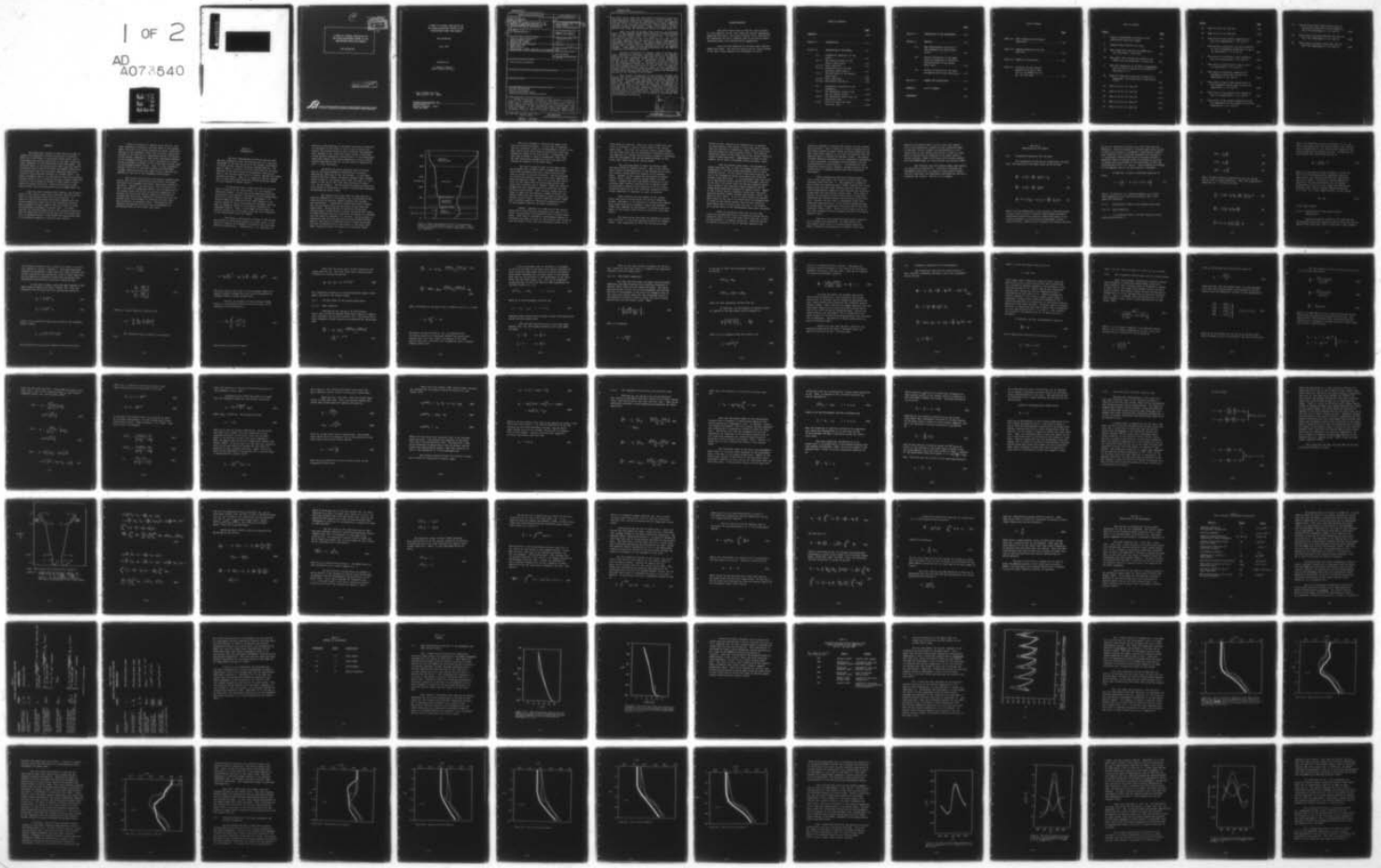

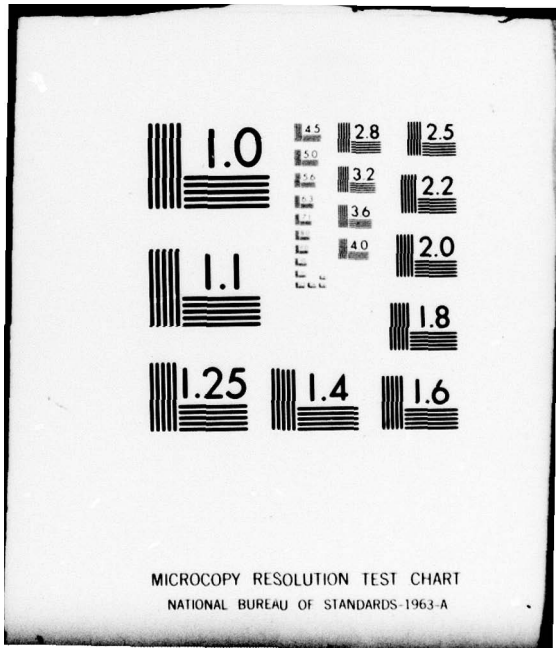
1.0
1.1
1.25
1.4
1.6
1.8
2.0
2.2
2.5
2.8
3.2
3.6
4.0
4.5
5.0
5.6
MICROCOPY RESOLUTION TEST CHART
NATIONAL BUREAU OF STANDARDS-1963-A

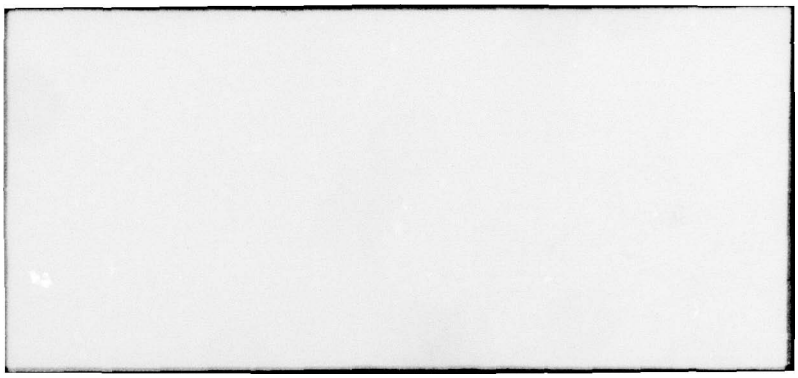

(12)

A MODEL OF DIURNAL VARIABILITY OF THE OCEAN-ATMOSPHERE SYSTEM IN THE UNDISTURBED TRADE WIND REGIME

SAI-79-807-WA

SAI
ATLANTA • ANN ARBOR • BOSTON • CHICAGO • CLEVELAND • DENVER • HUNTSVILLE • LA JOLLA
LITTLE ROCK • LOS ANGELES • SAN FRANCISCO • SANTA BARBARA • TUCSON • WASHINGTON

A MODEL OF DIURNAL VARIABILITY OF THE OCEAN-ATMOSPHERE SYSTEM IN THE UNDISTURBED TRADE WIND REGIME

SAI-79-807-WA

July 1979

Prepared by:

R. Michael Clancy*
Ocean Science Division

* Now at NORDA Code 322
NSTL Station, MS 39529

SCIENCE APPLICATIONS, INC.
8400 Westpark Dr.
McLean, Virginia 22101
(703) 821-4300

UNCLASSIFIED

SECURITY CLASSIFICATION OF THIS PAGE (When Data Entered)

REPORT DOCUMENTATION PAGE		READ INSTRUCTIONS BEFORE COMPLETING FORM
1. REPORT NUMBER (14) SAI-79-807-WA	2. GOVT ACCESSION NO.	3. RECIPIENT'S CATALOG NUMBER (9)
4. TITLE (and Subtitle) (6) A MODEL OF DIURNAL VARIABILITY OF THE OCEAN-ATMOSPHERE SYSTEM IN THE UNDISTURBED TRADE WIND REGIME.		5. TYPE OF REPORT & PERIOD COVERED Final Report. 7/1 78 - Aug 79 2/78 - 8/79
		6. PERFORMING ORG. REPORT NUMBER
7. AUTHOR(s) (10) R. Michael Clancy		8. CONTRACT OR GRANT NUMBER(s) (15) N00014-78-C-0287
9. PERFORMING ORGANIZATION NAME AND ADDRESS Science Applications Inc. 8400 Westpark Drive McLean, VA 22102		10. PROGRAM ELEMENT, PROJECT, TASK AREA & WORK UNIT NUMBERS (11) Jul 79
11. CONTROLLING OFFICE NAME AND ADDRESS NORDA Code 322 NSTL Station Mississippi 39529 Attn Dr. S.A. Piacsek		12. REPORT DATE (12) 130p 13. NUMBER OF PAGES 123
14. MONITORING AGENCY NAME & ADDRESS(if different from Controlling Office)		15. SECURITY CLASS. (of this report) Unclassified 15a. DECLASSIFICATION/DOWNGRADING SCHEDULE

16. DISTRIBUTION STATEMENT (of this Report)

Distribution Unlimited

17. DISTRIBUTION STATEMENT (of the abstract entered in Block 20, if different from Report)

18. SUPPLEMENTARY NOTES

19. KEY WORDS (Continue on reverse side if necessary and identify by block number)

Air-Sea Interaction
Oceanic Mixed Layer
Planetary Boundary Layer
Cumulus Convection Parameterization

20. ABSTRACT (Continue on reverse side if necessary and identify by block number)

One-dimensional coupled air-sea models are used to compare the responses to diurnal heating of a diffusive model and a bulk model of the oceanic mixed layer, and to investigate the diurnal variability of the upper ocean and lower atmosphere in the undisturbed trade wind regime. The diffusive model of the oceanic mixed layer uses the Level-2 turbulence closure theory of Mellor and Yamada (1974) while

DD FORM 1 JAN 73 1473 EDITION OF 1 NOV 65 IS OBSOLETE S/N 0102-LF-014-6501

UNCLASSIFIED

SECURITY CLASSIFICATION OF THIS PAGE (When Data Entered)

411 104

JOB

Cont'

the bulk model uses the entrainment hypothesis and mean-turbulent-field modeling technique of Garwood (1977). The model atmosphere used in all experiments treats the planetary boundary layer in a bulk fashion and uses a highly simplified version of the Arakawa and Schubert (1973) theory to parameterize cumulus convection. Model verification is made against data from the undisturbed period of BOMEX Phase III.

Near the time of maximum solar heating, the diffusive model of the oceanic mixed layer maintains turbulent mixing down to a much greater depth than the bulk model. In addition, the diffusive model mixes heat supplied near the surface downward on some finite time scale while the bulk model assumes that heat supplied near the surface is mixed instantaneously throughout the mixed layer. For these reasons, the diffusive model gives a more accurate simulation than the bulk model during the day when the net surface heat flux is changing rapidly. Both models give good predictions of the observed temperature profiles near sunrise.

Diurnal variations of cumulus cloud activity, low-level temperature, moisture, and wind speed in the coupled-model are found to be forced primarily by direct radiational heating of the atmosphere rather than by direct radiational heating of the ocean and its associated diurnal fluctuation in sea surface temperature. The direct radiational heating of the atmosphere forces the diurnal fluctuation in cloud activity through its effect on the "cloud layer forcing term" of the Arakawa-Schubert theory. This, in turn, produces a diurnal variation in low-level moisture and wind speed through cloud-related vertical eddy fluxes of moisture and momentum at the top of the atmospheric mixed layer.

The diurnal fluctuation of the surface sensible plus latent heat flux is controlled by both direct radiational heating of the atmosphere and direct radiational heating of the ocean. However, the amplitude of this fluctuation is about two orders of magnitude smaller than the amplitude of the surface solar flux which is primarily responsible for driving the diurnal sea surface temperature fluctuation. Although the sea surface temperature fluctuation alters the surface solar flux through its influence on cloud cover, this alteration is extremely small. Consequently, the feedback loop between the ocean and the atmosphere is exceedingly weak at the diurnal time scale.

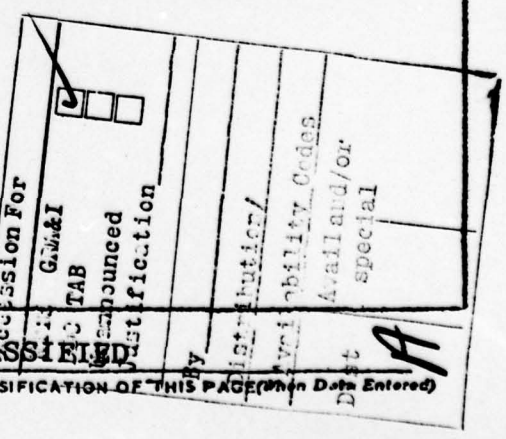

ACKNOWLEDGEMENTS

The author would like to thank Dr. Steve Piacsek, Dr. Glyn Roberts, and Dr. Burt Green for helpful suggestions regarding this work. He is also indebted to Mr. Paul Martin for supplying him with a computer code of the Mellor-Yamada turbulence model and offering useful suggestions.

This work was supported by the Navy under contract N00014-78-C-0287. The contract monitor was Dr. Steve Piacsek of the Naval Ocean Research and Development Activity.

TABLE OF CONTENTS

LIST OF TABLES

LIST OF FIGURES

ABSTRACT

One-dimensional coupled air-sea models are used to compare the responses to diurnal heating of a diffusive model and a bulk model of the oceanic mixed layer, and to investigate the diurnal variability of the upper ocean and lower atmosphere in the undisturbed trade wind regime. The diffusive model of the oceanic mixed layer uses the Level-2 turbulence closure theory of Mellor and Yamada (1974) while the bulk model uses the entrainment hypothesis and mean-turbulent-field modeling technique of Garwood (1977). The model atmosphere used in all experiments treats the planetary boundary layer in a bulk fashion and uses a highly simplified version of the Arakawa and Schubert (1973) theory to parameterize cumulus convection. Model verification is made against data from the undisturbed period of BOMEX Phase III.

Near the time of maximum solar heating, the diffusive model of the oceanic mixed layer maintains turbulent mixing down to a much greater depth than the bulk model. In addition, the diffusive model mixes heat supplied near the surface downward on some finite time scale while the bulk model assumes that heat supplied near the surface is mixed instantaneously throughout the mixed layer. For these reasons, the diffusive model gives a more accurate simulation than the bulk model during the day when the net surface heat flux is changing rapidly. Both models give good predictions of the observed temperature profiles near sunrise.

Diurnal variations of cumulus cloud activity, low-level temperature, moisture, and wind speed in the coupled-model are found to be forced primarily by direct radiational heating of the atmosphere rather than by direct radiational heating of the ocean and its associated diurnal fluctuation in sea surface temperature. The direct radiational heating of the atmosphere forces the diurnal fluctuation in cloud activity through its effect on the "cloud layer forcing term" of the Arakawa-Schubert theory. This, in turn, produces a diurnal variation in low-level moisture and wind speed through cloud-related vertical eddy fluxes of moisture and momentum at the top of the atmospheric mixed layer.

The diurnal fluctuation of the surface sensible plus latent heat flux is controlled by both direct radiational heating of the atmosphere and direct radiational heating of the ocean. However, the amplitude of this fluctuation is about two orders of magnitude smaller than the amplitude of the surface solar flux which is primarily responsible for driving the diurnal sea surface temperature fluctuation. Although the sea surface temperature fluctuation alters the surface solar flux through its influence on cloud cover, this alteration is extremely small. Consequently, the feedback loop between the ocean and the atmosphere is exceedingly weak at the diurnal time scale.

Section 1
INTRODUCTION

The Naval Oceanographic Prediction System (OPS) has been proposed to meet the growing need for a detailed knowledge of the time evolution of the oceanic environment in which various acoustic detection systems operate. The goal of OPS is to provide five-day predictions of the major features of the world ocean with reasonable accuracy and detail, and two-day predictions for smaller regions with higher accuracy and detail. When it is completed, OPS will become part of the Primary Environmental Processing System (PEPS) at Fleet Numerical Weather Central.

At any given time, a large fraction of the world ocean is covered by the undisturbed (i.e. fair weather) trade wind regime. On the time scale associated with OPS, the period of the dominant fluctuations in the thermodynamic structure of this system is diurnal. Furthermore, as noted by Shonting (1964) and Urick (1975) Chapter 1, the diurnal change in the stratification of the upper ocean can have an important effect on the acoustic detection of submerged objects. Thus, in this paper we will model the diurnal variability of the upper ocean and lower atmosphere in the undisturbed trade wind regime.

This study is additionally relevant to OPS because the success of the program depends to a great extent on our ability to deduce the atmospheric forcing of the ocean from satellite observations. Consequently, it is important to

develop an understanding of the short-time-scale variability of processes on both sides of the air-sea interface that control the surface fluxes of heat, moisture, and momentum. Also, because of the relatively large diurnal fluctuation in sea surface temperature characteristic of the undisturbed trade wind regime, this region represents an area in which interactions between the air and sea could be important on the 1 - 5 day time scale.

We define the marine boundary layer to be that part of the ocean-atmosphere system which is directly affected by conditions at the sea surface. In the undisturbed trade wind regime, the marine boundary layer extends from the base of the oceanic mixed layer (at about 5 - 50 m depth) to the top of the trade wind inversion (at about 1.5 - 2.5 km height). The well-defined layered structure of this system is illustrated in Figure 1 and has been discussed by Garstang and Betts (1974).

The oceanic mixed layer owes its high degree of vertical homogeneity to turbulence that is generated by the wind and the intermittent upward buoyancy flux through the sea surface. A dynamically stable water mass in which the vertical eddy fluxes are very small exists below the mixed layer. During periods of relatively strong wind forcing and/or strong surface cooling, the mixed layer tends to deepen because the more dense water from below is entrained into the layer by turbulence at its base. During periods of relatively weak wind forcing and/or strong surface heating, however, the source of turbulent kinetic energy may become too weak to maintain active entrainment at the mixed layer base, causing the layer to retreat to a shallower depth.

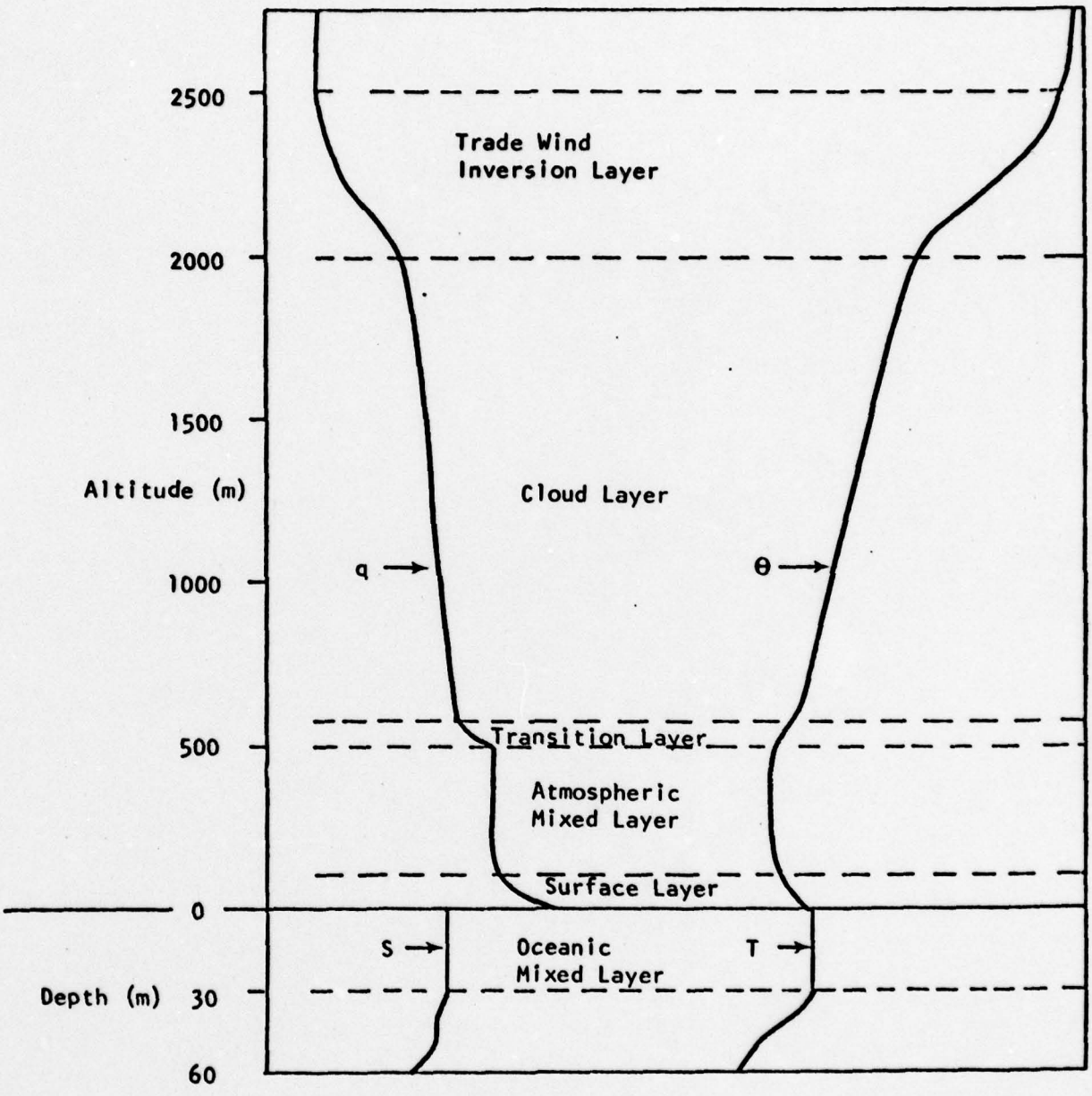

Figure 1. Typical thermodynamic structure of the undisturbed trade wind regime (note change of scale at sea surface). Here q is water vapor mixing ratio, θ potential temperature, S salinity, and T temperature.

The first attempts at modeling the upper ocean were with diffusive models. In this type of approach, vertical turbulent fluxes are parameterized in terms of the mean fields using eddy diffusion coefficients which may themselves depend on the mean fields. An advantage of this type of model is that no assumptions (other than the eddy coefficient assumption) need to be made concerning the behavior of the mixed layer.

The first diffusive model of the upper ocean was probably that of Ekman (1905) although this formulation was concerned only with current structure and took no account of density structure. The two problems of current and density structure were first combined by Munk and Anderson (1948). The forms of the eddy coefficient in this model were determined empirically from stratified turbulence data. Mamayev (1958) and Pandolfo (1969) have also proposed empirical forms for the eddy diffusion coefficients. More recently, models such as those of Vager and Zilitinkevich (1968) and Mellor and Yamada (1974) have been developed in light of modern turbulence closure theory. Martin (1976) and Jacobs (1978) have performed numerical experiments comparing several of the proposed forms for the eddy coefficients.

Another approach is to make use of the oceanic mixed layer's near vertical homogeneity and model it as a "slab" in which mean field quantities have no depth dependence. This type of treatment is advantageous because it eliminates the need to solve for the interior eddy fluxes as only the surface fluxes and the entrainment fluxes at the

layer base are required. Kraus and Turner (1967) were the first to construct a slab or "bulk" model of the oceanic mixed layer. They used the turbulent kinetic energy budget for the mixed layer and the approximately decoupled state of the equations for thermal and mechanical energies to determine both the entrainment rate during deepening phase and the mixed layer depth during the retreat phase.

The prototype model of Kraus and Turner (1967) has been refined by several authors. Most of the refinements involve parameterization of the dissipation of turbulent kinetic energy which was ignored in the original model. Notable in this regard are the efforts of Denman (1973), Niiler (1975), Elsberry et al. (1976), and Kim (1976). Probably the most significant alteration of the protoype model, however, has been that of Garwood (1977) in which mean-turbulent-field modeling of the vertically integrated equations for the individual turbulent kinetic energy components is employed to close the problem.

Both diffusive and bulk models of the oceanic mixed layer may be incorporated into various components of OPS. Therefore, it is important to evaluate and compare their short-time-scale responses. Martin and Thompson (1978) have compared the performance of diffusive and bulk models of the oceanic mixed layer on relatively long time scales.

The theory which describes the atmospheric surface layer (see Fig. 1) was first advanced by Monin and Obukhov (1954). They recognized the fact that the vertical eddy

fluxes of heat, moisture, and momentum can be regarded as quasi-constant with height in this layer which implies that the profiles of temperature, water vapor mixing ratio, and wind speed will have universal forms. This powerful similarity theory allows prediction of the surface fluxes in terms of mean quantities. Comprehensive reviews of this subject can be found in Businger (1975) and Busch (1977).

Like the oceanic mixed layer, the atmospheric mixed layer (see Fig. 1) owes its tendency toward vertical homogeneity to vertical mixing associated with its fully turbulent nature. In the typical trade wind situation, the top of the atmospheric mixed layer occurs just below the average cloud base level. It is maintained, near this level by an approximate balance between the entrainment velocity at the top of the mixed layer and the mean downward motion there caused by the large-scale mass divergence and the compensating subsidence produced by cumulus clouds. Models of the tropical marine atmospheric mixed layer have been proposed by Betts (1973), Arakawa and Schubert (1974), and Ogura and Cho (1974). In all of these studies the entrainment fluxes at the top of the mixed layer are parameterized in terms of the surface fluxes, and the thin transition layer which tops the mixed layer (see Fig. 1) is treated as a discontinuity in the thermodynamic mean field variables.

Below the transition layer the vertical eddy fluxes are accomplished mainly by mechanical mixing and dry convection while in the cloud layer above (see Fig. 1) they are due primarily to cumulus convection. Parameterization of cumulus convection is one of the most important and

difficult problems in tropical meteorology and has received much attention. Early attempts at cumulus parameterization have been reviewed by Ogura (1972) and Bates (1972) but the most significant advance in this area has probably been the spectral model of Arakawa and Schubert (1974). This model included important processes such as compensating subsidence in the environment, entrainment and detrainment, and the re-evaporation of cloud droplets. It provided the first closed and theoretically rigorous, parameterization of the interaction of a cumulus ensemble with the large-scale environment.

While condensation generally exceeds evaporation in the cloud layer, the reverse is true of the trade inversion layer (see Fig. 1). The diagnostic studies of Nitta (1975) and Soong and Ogura (1976) indicate that clouds penetrating into the trade inversion detrain liquid water (which subsequently evaporates) and saturated air creating a strong heat sink and moisture source there. This tends to balance the heating and drying effects due to large-scale subsidence and thereby maintain the structure of the inversion. Finally, we note that in undisturbed trade wind conditions practically all of the clouds originating from the mixed layer are confined to below the top of the trade inversion (Nitta, 1975). Hence, in this case, the top of the trade inversion can be considered the top of the marine boundary layer.

Because of its relatively high degree of horizontal uniformity and steadiness, the undisturbed trade wind region lends itself to one-dimensional modeling. Hence, following the precedents of Pandolfo (1971) and

Pandolfo and Jacobs (1972), we will study this regime with a one dimensional, coupled air-sea, numerical model. In addition, we will compare the performance of a diffusive model of the oceanic mixed layer to that of a bulk model in simulating the response of the upper ocean to diurnal heating. Model verification will be made against data from BOMEX Phase III (see Kuettner and Holland, 1969).

The diffusive and bulk oceanic mixed layer models are described in Section 2.1. Section 2.2 develops the atmospheric model that is coupled to both oceanic models. Section 3 describes the experiments performed and Section 4 discusses the results. Section 5 is a summary.

Section 2
DESCRIPTION OF THE MODELS

2.1. Fundamental Equations for the Ocean

The fundamental equations for conservation of heat, salt, and momentum in the upper ocean can be written

$$\frac{\partial \overline{T}}{\partial t} = - \underset{\sim}{\overline{v}} \cdot \overline{\nabla_z T} - \overline{w} \frac{\partial \overline{T}}{\partial z} - \frac{\partial}{\partial z} \overline{w' T'} + \overline{Q}_R \qquad (1)$$

$$\frac{\partial \overline{S}}{\partial t} = - \underset{\sim}{\overline{v}} \cdot \overline{\nabla_z S} - \overline{w} \frac{\partial \overline{S}}{\partial z} - \frac{\partial}{\partial z} \overline{w' S'} \qquad (2)$$

$$\frac{\partial \underset{\sim}{\overline{v}}}{\partial t} = f \hat{k} \times (\underset{\sim}{\overline{v}} - \underset{\sim}{\overline{v}}_g) - (\underset{\sim}{\overline{v}} \cdot \nabla_z) \underset{\sim}{\overline{v}} - \overline{w} \frac{\partial \underset{\sim}{\overline{v}}}{\partial z} - \frac{\partial}{\partial z} \overline{w' \underset{\sim}{v}'} \qquad (3)$$

where T is the temperature, S the salinity, $\underset{\sim}{v}$ the horizontal current velocity vector (standard right-handed Cartessian coordinate system with z positive upward and origin at sea surface assumed), $\underset{\sim}{v}_g$ the horizontal geostrophic current velocity vector, w the vertical component of current velocity,

Q_R the net radiational heating rate, and f the Coriolis parameter. Spatial averages at constant depth taken across a region large enough to encompass a statistically significant sampling of all unresolved phenomena are denoted by $(\bar{})$ and primes indicate departures from these averages. Gradients taken at constant depth are denoted by (∇_z) and we assume that fluctuations in the horizontal current are uncorrelated with T', S', and $\underset{\sim}{v}'$. Other symbols are defined in the Appendix and all of the notation is standard.

In addition, we have a linearized equation of state

$$\rho = \rho_w \left[1 - \alpha (T - T_w) + \beta (S - S_w)\right] \tag{4}$$

where ρ is density, ρ_w a reference density, T_w a reference temperature, S_w a reference salinity, and α and β empirical constants.

2.1.1. The Diffusive Model of the Oceanic Mixed Layer

2.1.1.1. Basic Equations

In a diffusive model, the eddy fluxes are parameterized according to

$$\overline{w'T'} = - K_H \frac{\partial \bar{T}}{\partial z} \tag{5}$$

$$\overline{w'S'} = - K_S \frac{\partial \bar{S}}{\partial z} \tag{6}$$

$$\overline{w'\underset{\rightarrow}{v}'} = - K_M \frac{\partial \bar{\underset{\rightarrow}{v}}}{\partial z} \tag{7}$$

where the eddy diffusion coefficients, K_H, K_S, and K_M may be time- and space-dependent. Thus, the conservation equations (1) - (3) can be written

$$\frac{\partial \bar{T}}{\partial t} = - \bar{\underset{\rightarrow}{v}} . \overline{\nabla_z T} + \frac{\partial}{\partial z} \left(K_H \frac{\partial \bar{T}}{\partial z} \right) - \frac{I_o}{\rho_w c} \frac{\partial}{\partial z} e^{\gamma z} \tag{8}$$

$$\frac{\partial \bar{S}}{\partial t} = - \bar{\underset{\rightarrow}{v}} . \overline{\nabla_z S} + \frac{\partial}{\partial z} \left(K_S \frac{\partial \bar{S}}{\partial z} \right) \tag{9}$$

$$\frac{\partial \underset{\rightarrow}{v}}{\partial t} = f\hat{k} \times \bar{\underset{\rightarrow}{v}} + \frac{\partial}{\partial z} \left(K_M \frac{\partial \bar{\underset{\rightarrow}{v}}}{\partial z} \right) - D\bar{\underset{\rightarrow}{v}} \tag{10}$$

where, for simplicity we have assumed $\overline{v}_g = \overline{w} = 0$. We have also assumed that the Rossby number of the horizontally averaged flow is $<<1$, which allows neglect of the lateral advection of momentum in (10). In addition, we have modeled the radiational heating as

$$\bar{Q}_R = -\frac{I_o}{\rho_w c}\frac{\partial}{\partial z} e^{\gamma z} \tag{11}$$

where c is the specific heat of seawater, I_o the surface flux of penetrating solar radiation (positive upward) and γ an extinction coefficient (see Niiler and Kraus, 1975). Furthermore, we have modeled the damping of inertial oscillations due to downward propagation of internal wave energy (see Pollard and Millard, 1970) with a constant damping coefficient D in (10). As a final simplification, we will assume

$$K_S = K_H \tag{12}$$

in all that follows.

2.1.1.2 Determination of the Eddy Diffusion Coefficients

Through systematic scaling of the equations for the Reynolds fluxes and turbulent kinetic energy, Mellor and Yamada (1974) developed a set of turbulence closure models

for planetary boundary layers labeled, in order of increasing complexity, Levels 1 through 4. They used hypotheses proposed by Kolmogoroff (1942) and Rotta (1951) to model the triple correlation and dissipation terms in these equations and the empirical constants arising from the theory were determined from neutrally stratified turbulence data.

In the Level 2 model, which has been applied to the upper ocean by Mellor and Durbin (1975), (8) - (10) are recovered with the eddy diffusion coefficients given by

$$K_H = \ell \left(2 \overline{E}\right)^{1/2} A_H \tag{13}$$

$$K_M = \ell \left(2 \overline{E}\right)^{1/2} A_M \tag{14}$$

where ℓ is a turbulence length scale and $\overline{E}$ is the turbulent kinetic energy

$$\overline{E} \equiv \tfrac{1}{2} \overline{\left(u'^2 + v'^2 + w'^2\right)} \tag{15}$$

The quantities A_H and A_M are stability functions given by

$$A_H = n_1 - \frac{n_2 R_f}{(1-R_f)} \tag{16}$$

$$A_M = A_H \frac{\left(n_3 - \frac{n_4 R_f}{(1-R_f)}\right)}{\left(n_5 - \frac{n_6 R_f}{(1-R_f)}\right)} \tag{17}$$

where $n_1 - n_6$ are empirical constants and

$$R_f \equiv \frac{A_H}{A_M} \left[\frac{g}{\rho_w} \frac{\partial \bar{\rho}}{\partial z} \left| \frac{\partial \bar{\vec{v}}}{\partial z} \right| -2 \right]$$

The turbulent kinetic energy $\bar{E}$ is calculated from

$$0 = K_M \left| \frac{\partial \bar{\vec{v}}}{\partial z} \right|^2 - K_H g \left[\alpha \frac{\partial \bar{T}}{\partial z} - \beta \frac{\partial \bar{S}}{\partial z} \right] - n_7 \bar{E}^{3/2} \qquad (18)$$

The three terms on the right of (18) represent shear production, buoyant dissipation, and viscous dissipation of turbulent kinetic energy respectively.

Finally, an estimate of the turbulence length scale, ℓ, is calculated from the vertical extent of the turbulence field according to

$$\ell = \frac{n_8 \int_{-\infty}^{0} z \bar{E}^{1/2} \, dz}{\int_{-\infty}^{0} \bar{E}^{1/2} \, dz} \qquad (19)$$

which closes the diffusive model.

Note that the mixed layer is here defined as the region where $\bar{E} > 0$. Below the mixed layer, weak vertical diffusion is retained by setting

$$K_H = K_S = K_M = 1 \times 10^{-4} \ m^2 s^{-1} \tag{20}$$

For a detailed discussion of the scaling which leads to this model, see Mellor and Yamada (1974).

2.1.2 The Bulk Model of the Oceanic Mixed Layer

2.1.2.1 Basic equations

Defining T_m, S_m, and $\underline{v}_m$ to be the horizontally- and vertically-averaged mixed-layer values of temperature, salinity, and current velocity, (1) - (3) can be vertically averaged to yield conservation equations for these quanties

$$\frac{\partial T_m}{\partial t} = - (\bar{\underline{v}} \cdot \overline{\nabla_z T})_M - \frac{\left| \overline{(w'T')}_o - \overline{(w'T')}_{-h} \right|}{h}$$

$$- \frac{I_o}{\rho_w c h} (1 - e^{-\gamma h}) \tag{21}$$

$$\frac{\partial S_m}{\partial t} = -(\bar{\underset{\sim}{v}} \cdot \overline{\nabla_z S})_M - \frac{\left|(\overline{w'S'})_o - (\overline{w'S'})_{-h}\right|}{h} \qquad (22)$$

$$\frac{\partial \underset{\sim}{v}_m}{\partial t} = f\hat{k}X(\bar{\underset{\sim}{v}} - \bar{\underset{\sim}{v}}_g)_M - \frac{\left|(\overline{w'\underset{\sim}{v}'})_o - (\overline{w'\underset{\sim}{v}'})_{-h}\right|}{h} - D\underset{\sim}{v}_m \qquad (23)$$

where the bottom of the mixed layer is taken to be at $z = -h$ and

$$(\ )_M \equiv \frac{1}{h}\int_{-h}^{o} (\ )dz$$

As before, we have assumed $\bar{w} = \bar{v}_g = 0$, neglected the horizontal advection of momentum, modeled the radiational heating with (11), and treated the damping of the mean motion field due to internal wave propagation with a constant damping coefficient.

A thin entrainment zone of thickness δ is assumed to exist at the base of the mixed layer which separates the fully turbulent water above from the relatively quiescent water below. Assuming that the eddy fluxes in the entrainment zone are due entirely to the entrainment of the lower fluid into the mixed layer, (1) - (3) can be integrated across the zone to yield the familiar jump expressions for the eddy fluxes at $z = -h$

$$(\overline{w'\zeta'})_{-h} = -\Delta\zeta w_e \qquad \zeta = T, S, \underline{\chi} \tag{24}$$

where w_e is the entrainment velocity and

$$\Delta\zeta = \zeta_{-h} - \zeta_{-h-\delta} \qquad \zeta = \bar{T}, \bar{S}, \bar{\underline{\chi}} \tag{25}$$

represent quasi-discontinuous changes in mean field quantities across the entrainment zone.

With the mean vertical motion at the layer base assumed zero, the relationship between w_e and layer depth is simply

$$w_e = \frac{\partial h}{\partial t} \qquad \text{for} \quad \frac{\partial h}{\partial t} > 0$$

$$w_e = 0 \qquad \text{for} \quad \frac{\partial h}{\partial t} \leq 0 \tag{26}$$

Thus, as the layer becomes shallower all entrainment ceases and the mixed layer is assumed to be completely decoupled from the region below.

2.1.2.2 Entrainment Hypothesis

To close the bulk model, we adopt the entrainment hypothesis and mean-turbulent-field modeling technique of Garwood (1977) which will be summarized below. The basic assumption here is that the critical parameter determining the rate of entrainment is the ratio P of buoyancy flux at the layer base (which stabilizes the entrainment zone) to convergence of turbulent kinetic energy flux there (which destabilizes the entrainment zone). Thus,

$$P = \left[\frac{\overline{b'w'}}{\frac{\partial}{\partial z}\left[\overline{w'\left(\frac{E}{2} + \frac{p'}{\rho_w}\right)}\right]} \right]_{-h} \tag{27}$$

where b is buoyancy

$$b \equiv g \frac{(\rho_w - \rho)}{\rho_w} \tag{28}$$

In analogy to (23), the entrainment buoyancy flux can be written

$$(\overline{b'w'})_{-h} = -\Delta b w_e \tag{29}$$

or

$$(\overline{b'w'})_{-h} = -\left|\alpha\Delta T - \beta\Delta S\right| w_e \tag{30}$$

where the last expression follows from (4).

In addition, the convergence of turbulent kinetic energy in the entrainment zone is modeled as

$$\frac{-\partial}{\partial z}\left[\overline{w'\left(\frac{E}{2} + \frac{p'}{\rho_w}\right)}\right]_{-h} = \frac{(\bar{E})_M}{\tau_e} \tag{31}$$

where τ_e is a transport time scale taken to be

$$\tau_e = a_1 h(\overline{w'^2})_M^{-1/2} \tag{32}$$

and a_1 is a proportionality constant. Assigning the critical constant parameter P the value of m_4 (following Garwood's notation), (27) and (30) - (32) can be combined to yield an entrainment equation

$$\frac{\partial h}{\partial t} = \frac{m_4(\bar{E})_M \ (\overline{w'^2})_M^{1/2}}{a_1 \ h\left|\alpha\Delta T - \beta\Delta S\right|} \quad \text{for} \quad \frac{\partial h}{\partial t} > 0 \qquad (33)$$

To close the model, the integral over mixed layer depth of generation, redistribution, and viscous dissipation of turbulent kinetic energy are parameterized and a quasi-steady-state assumption for turbulent kinetic energy invoked. Then, (33) and the budget equations for the individual components of turbulent kinetic energy can be solved for $\partial h/\partial t$ during the deepening phase. During the retreat phase, the entrainment rate is identically zero which allows h to be determined diagnostically from the same set of equations. The details of these calculations are given by Garwood (1977).

Finally, we note that the heat, salinity, and momentum fields below the base of the mixed layer are again calculated from (8) - (10) and (20).

2.2 Fundamental Equations for the Atmosphere

The fundamental equations for conservation of heat, moisture, momentum, and mass in the lower atmosphere can be written

$$\frac{\partial \tilde{s}}{\partial t} = -\tilde{\underset{\rightarrow}{v}} \cdot \widetilde{\nabla_p s} - \tilde{\omega} \frac{\partial \tilde{s}}{\partial p} - \frac{\partial}{\partial p} \widetilde{\omega' s'} + L_v \tilde{Q}_c + \tilde{Q}_R \tag{34}$$

$$\frac{\partial \tilde{q}}{\partial t} = -\tilde{\underset{\rightarrow}{v}} \cdot \widetilde{\nabla_p q} - \tilde{\omega} \frac{\partial \tilde{q}}{\partial p} - \frac{\partial}{\partial p} \widetilde{\omega' q'} - \tilde{Q}_c \tag{35}$$

$$\frac{\partial \tilde{\underset{\rightarrow}{v}}}{\partial t} = f\hat{k}X(\tilde{\underset{\rightarrow}{v}} - \tilde{\underset{\rightarrow}{v}}_g) - (\tilde{\underset{\rightarrow}{v}} \cdot \nabla_p)\tilde{\underset{\rightarrow}{v}} - \tilde{\omega} \frac{\partial \tilde{\underset{\rightarrow}{v}}}{\partial p} - \frac{\partial}{\partial p} \widetilde{\omega' \underset{\rightarrow}{v}'} \tag{36}$$

$$\nabla_p \cdot \tilde{\underset{\rightarrow}{v}} + \frac{\partial \tilde{\omega}}{\partial p} = 0 \tag{37}$$

where s is the dry static energy given by

$$s = c_p T + gz,$$

q the water vapor mixing ratio (mass of water vapor per mass of dry air), $\underset{\sim}{v}$ the wind velocity vector projected on a surface of constant pressure, p the pressure, ω the vertical p-velocity ($\omega = dp/dt$), Q_R the net radiational heating rate, and Q_C the rate of condensation minus evaporation per unit mass of air. Spatial averages at constant pressure taken across a region large enough to encompass a statistically significant sampling of all unresolved phenomena are denoted by (~) and primes indicate departures from these averages. Gradients taken at constant pressure are denoted by (∇_p) and we assume that fluctuations in $\underset{\sim}{v}$ are uncorrelated with s', q', and $\underset{\sim}{v}'$. Other symbols are defined in the Appendix and all of the notation is standard.

In addition, we have the hydrostatic equation

$$\frac{\partial \tilde{p}}{\partial z} = -\tilde{\rho} g \tag{39}$$

and an approximate equation of state for moist air

$$\frac{p}{\tilde{\rho}} = R\tilde{T}(1 + 0.61\tilde{q}) \tag{40}$$

where ρ is the density of moist air and R the gas constant.

2.2.1 The Atmospheric Surface Layer and the Surface Fluxes

Under quasi-steady, convectively unstable, horizontally homogeneous conditions, Monin-Obukhov similarity theory predicts that a surface layer of thickness -L exists in which the vertical eddy fluxes depart little from their surface values, and properly scaled vertical derivatives of temperature, moisture, and momentum are universal functions of z/L. Here, z is height above the surface and L is the Monin-Obukhov length, given to good approximation by (see Kraus, 1972)

$$L = \frac{\rho_a u_*^3}{\kappa \left[\frac{(\widetilde{\omega' s'})_o}{c_p T_a} + 0.61 \, (\widetilde{\omega' q'})_o \right]} \tag{41}$$

where κ is von Karmen's constant, ρ_a a reference density for air, T_a a reference temperature for air, and u_* the surface friction velocity in the air given by

$$u_* = \left(\frac{|\tau_o|}{\rho_a} \right)^{1/2} \tag{42}$$

with $\underset{\rightarrow}{\tau}_o$ the surface wind stress vector given by

$$\underset{\rightarrow}{\tau}_o = \frac{(\widetilde{\omega' \underset{\rightarrow}{v}'})_o}{g} \tag{43}$$

Using the fact that the surface layer is a quasi-constant flux layer and denoting quantities evaluated at the sea surface with the subscript o we have to good approximation

$$\left.\begin{aligned} \widetilde{\omega's'} &= (\widetilde{\omega's'})_o \\ \widetilde{\omega'q'} &= (\widetilde{\omega'q'})_o \\ \widetilde{\omega'u'} &= (\widetilde{\omega'u'})_o \\ \widetilde{\omega'v'} &= (\widetilde{\omega'v'})_o \end{aligned}\right\} \quad \text{for } p_o \geq p \geq p_a \tag{44}$$

where p_a is the pressure at the top of the surface layer which is taken to be at an altitude of $|L|$ above the surface.

The Monin-Obukhov similarity theory gives rise to the following expressions

$$\frac{\partial \tilde{s}}{\partial z} = \frac{(\widetilde{\omega' s'})_o \, \phi_s(z/L)}{\rho_a g \, \kappa u_* z} \tag{45}$$

$$\frac{\partial \tilde{q}}{\partial Z} = \frac{(\widetilde{\omega' q'})_o \, \phi_q(z/L)}{\rho_a g \, \kappa u_* z} \tag{46}$$

$$\frac{\partial \tilde{U}}{\partial Z} = \frac{u_*}{\kappa z} \, \phi_m(z/L) \tag{47}$$

where U is wind speed and the ϕ functions are empirically determined, non-dimensional similarity functions. The forms of the ϕ functions have been reviewed by Hogstrom (1974) and it is generally accepted that most surface layer data are well represented by

$$\left.\begin{aligned} \phi_s &= \phi_q = (1 - 9\tfrac{z}{L})^{-1/2} \\ \phi_m &= (1 - 15\tfrac{z}{L})^{-1/4} \end{aligned}\right\} \text{ for } L < 0 \tag{48}$$

which are the forms used here. Using (48), the profile relations (45) - (47) can be integrated from z_o, (the surface roughness length, to z (see Paulson, 1970).

$$\tilde{s}(z) = s_o + \frac{(\widetilde{\omega' s'})_o}{\rho_a g \kappa u_*} \left[\ln\left(\frac{z}{z_o}\right) - 2\ln\left(\frac{1 + Y_\theta^2}{2}\right) \right] \tag{49}$$

$$\tilde{q}(z) = q_o + \frac{(\widetilde{\omega' q'})_o}{\rho_a g \kappa u_*} \left[\ln\left(\frac{z}{z_o}\right) - 2\ln\left(\frac{1 + Y_q^2}{2}\right) \right] \tag{50}$$

$$\tilde{U}(z) = U_o + \frac{u_*}{k} \left[\ln\left(\frac{z}{z_o}\right) - 2\ln\left(\frac{1 + Y_m}{2}\right) - \ln\left(\frac{1 + Y_m^2}{2}\right) + 2\tan^{-1} Y_m - 1/2\pi \right] \tag{51}$$

where s_o, q_o, and U_o are dry static energy, water vapor mixing ratio, and wind speed at z_o, and

$$Y_\theta = Y_q = (1 - 9\frac{z}{L})^{1/4} \tag{52}$$

$$Y_m = (1 - 15\frac{z}{L})^{1/4} \tag{53}$$

At the top of the surface layer, $\tilde{s}$, $\tilde{q}$, and $\tilde{U}$ are given to excellent approximation, by their mixed layer values (see Section 2.2.2). Thus, setting $z = -L$ in (49) - (53) yields after rearrangement

$$\widetilde{(\omega's')}_o = \frac{\kappa u_* \rho_a g(s_m - s_o)}{\left[\ln(\frac{-L}{z_o}) - 1.466\right]} \tag{54}$$

$$\widetilde{(\omega'q')}_o = \frac{\kappa u_* \rho_a g(q_m - q_o)}{\left[\ln(\frac{-L}{z_o}) - 1.466\right]} \tag{55}$$

$$u_* = \frac{\kappa(U_m - U_o)}{\left[\ln(\frac{-L}{z_o}) - 0.844\right]} \tag{56}$$

where the subscript m indicates values characteristic of the atmospheric mixed layer.

Following Clarke (1970) and others, we assume that the roughness length for sea surface is given by

$$z_o = \max \left(\frac{0.032 u_*^2}{g}, z_{min} \right) \tag{57}$$

where $z_{min} = 0.0015$ cm. We calculate s_o from

$$s_o = c_p T_o \tag{58}$$

where T_o is the sea surface temperature. For the diffusive model T_o is taken to be the temperature at the uppermost gridpoint in the ocean, while for the bulk model it is set equal to the mixed layer temperature. Thus, we neglect any surface skin temperature effects (see Grassl, 1976). We set q_o equal to 0.98 times the saturation value at the sea surface to account for the effect of salinity on vapor pressure (see Roll, 1965). We set U_o equal to the magnitude of the surface drift velocity which is approximated by (Kraus, 1977)

$$\underset{\rightarrow}{v}_o = \left(\frac{\rho_a}{\rho_w} \right)^{1/2} (\underset{\rightarrow}{v}_g)_o + \underset{\rightarrow}{v}_m$$

where $(\underset{\rightarrow}{v}_g)_o$ is the surface geostrophic wind vector and $\underset{\rightarrow}{v}_m$ is the mean current vector in the oceanic mixed layer.

Equations (41), and (52) - (57) are solved iteratively at each time step. Then, the surface sensible and latent heat fluxes (positive upward) are given by

$$H_o = \frac{-(\widetilde{\omega's'})_o}{g} \tag{59}$$

$$L_v Q_o = -L_v \frac{(\widetilde{\omega'q'})_o}{g} \tag{60}$$

where L_v is the latent heat of evaporation. The surface wind stress vector is assumed to be in the direction of the mixed layer wind velocity which implies

$$\underset{\rightarrow}{\tau}_o = \rho_a u_*^2 \frac{\underset{\rightarrow}{v}_m}{|\underset{\rightarrow}{v}_m|} \tag{61}$$

where here $\underset{\rightarrow}{v}_m$ indicates the wind velocity vector in the atmospheric mixed layer.

Then, the total surface eddy fluxes of heat, salinity, and momentum for the ocean are given by (see Niiler and Kraus, 1977)

$$\rho_w c(\overline{w'T'})_o = F_o + B_o - I_o + H_o + L_v Q_o \qquad (62)$$

$$\rho_w(\overline{w'S'})_o = S_o(P_o - Q_o) \qquad (63)$$

$$\rho_w(\overline{w'\underset{\rightarrow}{v}'})_o = -\underset{\rightarrow}{I}_o \qquad (64)$$

where F is the total solar radiation flux, B the infrared radiation flux, I the penetrating component of the solar flux, and P the precipitation rate. The subscript o indicates evaluation of quantities at the sea surface and all fluxes are taken positive upward. Note that implicit in (64) is the assumption of a fully-developed sea.

The surface radiative fluxes are related to cloud cover using the formulation of Wyrtki (1965)

$$F_o = F_i \left| 1 - 0.38(C + C^2) \right| \tag{65}$$

$$B_o = \varepsilon b_* T_o^4 (0.39 - 2.0 q_{10}^{1/2}) (1 - 0.56C^2) + 4\varepsilon b_* T_o^3 (T_o - T_{10}) \tag{66}$$

where F_i is the surface solar flux in the absence of clouds, C the fractional cloud cover, ε the infrared emissivity of the sea surface, b_* the Stefan-Boltzmann constant, q_{10} the water vapor mixing ratio at 10 m height, and T_{10} the air temperature at 10 m height. Finally, we follow the suggestion of Niiler and Kraus (1975) and take

$$I_o = 0.45 F_o \tag{67}$$

2.2.2 The Atmospheric Mixed Layer and Transition Layer

Defining s_m, q_m, and $\underset{\rightarrow}{v}_m$ to be the horizontally- and vertically-averaged mixed-layer values of dry static energy, water vapor mixing ratio, and wind velocity, (34) - (36) can be vertically averaged to yield conservation equations for these quantities

$$\frac{\partial s_m}{\partial t} = -(\tilde{\underset{\rightarrow}{v}} \cdot \widetilde{\nabla_p s})_{ab} - \frac{\left|(\widetilde{\omega' s'})_b - (\widetilde{\omega' s'})_a\right|}{p_b - p_a} + (\tilde{Q}_R)_{ab} \quad (68)$$

$$\frac{\partial q_m}{\partial t} = -(\tilde{\underset{\rightarrow}{v}} \cdot \widetilde{\nabla_p q})_{ab} - \frac{\left|(\widetilde{\omega' q'})_b - (\widetilde{\omega' q'})_a\right|}{p_b - p_a} \quad (69)$$

$$\frac{\partial \underset{\rightarrow}{v}_m}{\partial t} = f\hat{k}X(\tilde{\underset{\rightarrow}{v}} - \tilde{\underset{\rightarrow}{v}}_g)_{ab} - \frac{\left|(\widetilde{\omega' \underset{\rightarrow}{v}'})_b - (\widetilde{\omega' \underset{\rightarrow}{v}'})_a\right|}{p_b - p_a} \quad (70)$$

where p_b is the pressure at the top of the mixed layer and

$$(\ )_{ab} \equiv \frac{1}{(p_b - p_a)} \int_{p_a}^{p_b} (\ ) \, dp \qquad (71)$$

Note that the Rossby number of the horizontally averaged flow is assumed <<1 which allows neglect of the lateral advection of momentum in (70). In addition, following Arakawa and Schubert (1974) and others, we have neglected any condensation or evaporation occurring within the mixed layer. We mention here that the assumption of vertical homogeneity for momentum in the atmospheric mixed layer of the trade wind regime may not always be good because of baroclinic effects (Pennell and LeMone, 1974). However, for simplicity, we will overlook this detail in the present study.

The transition layer at the top of the atmospheric mixed layer is in certain ways analogous to the entrainment zone at the base of the oceanic mixed layer. Eddies in the mixed layer impinge on the bottom of the transition layer, overshoot slightly, and thus entrain air from above down into the mixed layer. Following many others, we will model the

transition layer as a discontinuity in mean field quantities at p_b. Thus, in analogy to (9), the eddy fluxes at p_b can be expressed as

$$(\widetilde{\omega'\zeta'})_b = -\Delta\zeta\omega_e \qquad \zeta = s, q, \underset{\sim}{v} \tag{72}$$

where ω_e is the entrainment vertical p-velocity and

$$\Delta\zeta = \tilde{\zeta}_{b^-} - \zeta_m \qquad \zeta = s, q, \underset{\sim}{v} \tag{73}$$

Here the subscript b^- indicates evaluation of a quantity just above the discontinuity at p_b (see Fig. 2) and we have assumed that $\tilde{Q}_R$ is continuous across the transition layer.

The usual method for determining ω_e is to assume that it is proportional to the surface buoyancy flux (see Arakawa and Schubert, 1974), but we will employ a new approach here. First, we write a prediction equation for p_b

$$\frac{\partial p_b}{\partial t} = \tilde{\tilde{\omega}}_b + \omega_e \tag{74}$$

where horizontal advection of mixed layer thickness has been ignored and $\tilde{\bar{\omega}}_b$ is the average vertical p-velocity in the environment between the clouds. From mass continuity we can write

$$\tilde{\omega}_b = \omega_b^* + (1 - \sigma)\tilde{\bar{\omega}}_b \tag{75}$$

where $\tilde{\omega}_b$ is the vertical p-velocity at p_b due to the large-scale mass convergence (see (37)), σ is the fraction of the model domain covered by active cumulus updrafts, and ω_b^* is the convective vertical p-velocity at p_b defined by

$$\omega_b^* = \sum_{i=1}^{M} (\omega_i^* \sigma_i) \tag{76}$$

with ω_i^* the vertical p-velocity inside the $i^{\underline{th}}$ cloud updraft, σ_i the fraction of the model domain covered by the ith cloud updraft, and M the total number of cloud updrafts. In the undisturbed trade wind regime, $\sigma << 1$ and $|\frac{\partial p_b}{\partial t}| << |\tilde{\bar{\omega}}_b|$

Thus, from (74) and (75) we have to very good approximation,

$$\omega_e = \omega_b^* - \tilde{\omega}_b \tag{77}$$

The large-scale vertical p-velocity $\tilde{\omega}_b$ will be regarded as an imposed large-scale forcing function for one-dimensional implementation of the model. The quantity ω_b^* will be determined from a simple parameterization given in the next section.

Finally, following Betts (1976) we set

$$p_b = p_L \tag{78}$$

where p_L is the pressure at the lifting condensation level. The lifting condensation level is the level at which a parcel with the thermodynamic properties of the mixed layer becomes saturated when it is raised adiabatically from the surface. In the tropics it generally occurs very near cloud base. Thus, our conceptual model is that the height of the top of the mixed layer is controlled by the height of cloud base. This is a good model for the undisturbed trade wind regime, but it looses its validity in subtropical latitudes because cloud base often falls below the top of the mixed layer there, yielding a mixed layer that is topped by a solid deck of stratocumulus clouds (see Schubert, 1976).

2.2.3 The Cloud Layer and Trade Inversion Layer

Modeling the thermodynamics of the cloud layer and trade inversion layer is very difficult because, in addition to vertical eddy fluxes, subgrid-scale condensation and evaporation must also be parameterized. The theory of Arakawa and Schubert (1974) provides a closed parameterization of these eddy fluxes and source-sink terms but, even though their model contains many simplifying assumptions, it is still extremely complicated and predicts more than we are interested in here.

A simpler model is appropriate for the short time scale air-sea interaction problem since the main concern in this case is prediction of conditions near the surface rather than the details of the interaction between the cumulus ensemble and the large-scale environment which occurs primarily in the cloud and trade inversion layers. One way to simplify the problem is to make some assumption about the pressure dependence of s and q between the top of the transition layer and the top of the trade inversion and integrate (34) and (35) with respect to pressure in this region. The advantage of this is, of course, that knowledge of the specific pressure dependence of $\widetilde{\omega's'}$, $\widetilde{\omega'q'}$, and $\widetilde{Q}_c$ in the cloud layer and trade inversion is unnecessary. An approach similar to this has been taken by Albrecht (1977) who assumed a linear variation with respect to pressure of $\widetilde{s}$ and $\widetilde{q}$ in the cloud layer and modeled the trade inversion as a discontinuity in $\widetilde{s}$ and $\widetilde{q}$.

We will assume

$$\left.\begin{aligned} \tilde{s} &= \tilde{s}_{b^-} + \frac{(\tilde{s}_b - \tilde{s}_c)}{(p_{b^-} - p_c)} (p - p_{b^-}) \\ \tilde{q} &= \tilde{q}_{b^-} + \frac{(\tilde{q}_{b^-} - \tilde{q}_c)}{(p_{b^-} - p_c)} (p - p_{b^-}) \end{aligned}\right\} \text{for } p_{b^-} \geq p \geq p_c \tag{79}$$

and

$$\left.\begin{aligned} \tilde{s} &= \tilde{s}_d + \left(\frac{\partial \tilde{s}}{\partial p}\right)_I (p - p_d) \\ \tilde{q} &= \tilde{q}_d + \left(\frac{\partial \tilde{q}}{\partial p}\right)_I (p - p_d) \end{aligned}\right\} \text{for } p_c \geq p \geq p_d \tag{80}$$

where the subscripts b⁻, c, and d indicate evaluation of quantities at the top of the transition layer, base of the trade inversion, and top of the trade inversion, respectively (see Fig. 2) The quantities $(\partial\tilde{s}/\partial\tilde{p})I$ and $(\partial\tilde{q}/\partial\tilde{p})I$ are the vertical derivatives of $\tilde{s}$ and $\tilde{q}$ in the trade inversion layer and, along with $\tilde{s}_d$ and $\tilde{q}_d$, will be specified constants. Thus, in a way, we follow the lead of Ogura and Cho (1974) by topping the model with imposed profiles for s and q. In this case, however, the region where the profiles are imposed is the trade inversion and not the cloud layer, as is the case for the model of Ogura and Cho. Imposing a constant stratification in the trade inversion is appropriate for the problem considered here since experiments with the model have shown that reasonably large diurnal variations of the thermodynamic characteristics of the trade inversion have a negligible impact on the surface fluxes. Finally, we note that the assumed linear variations of $\tilde{s}$ (which implies nearly linear variations of temperature and potential temperature) and $\tilde{q}$ with respect to pressure are good approximations to the observations (e.g. Augstein et al. (1974), Soong and Ogura (1976), Esbensen (1978)).

Now, using (79) and (80), (34) and (35) can be integrated over pressure to yield

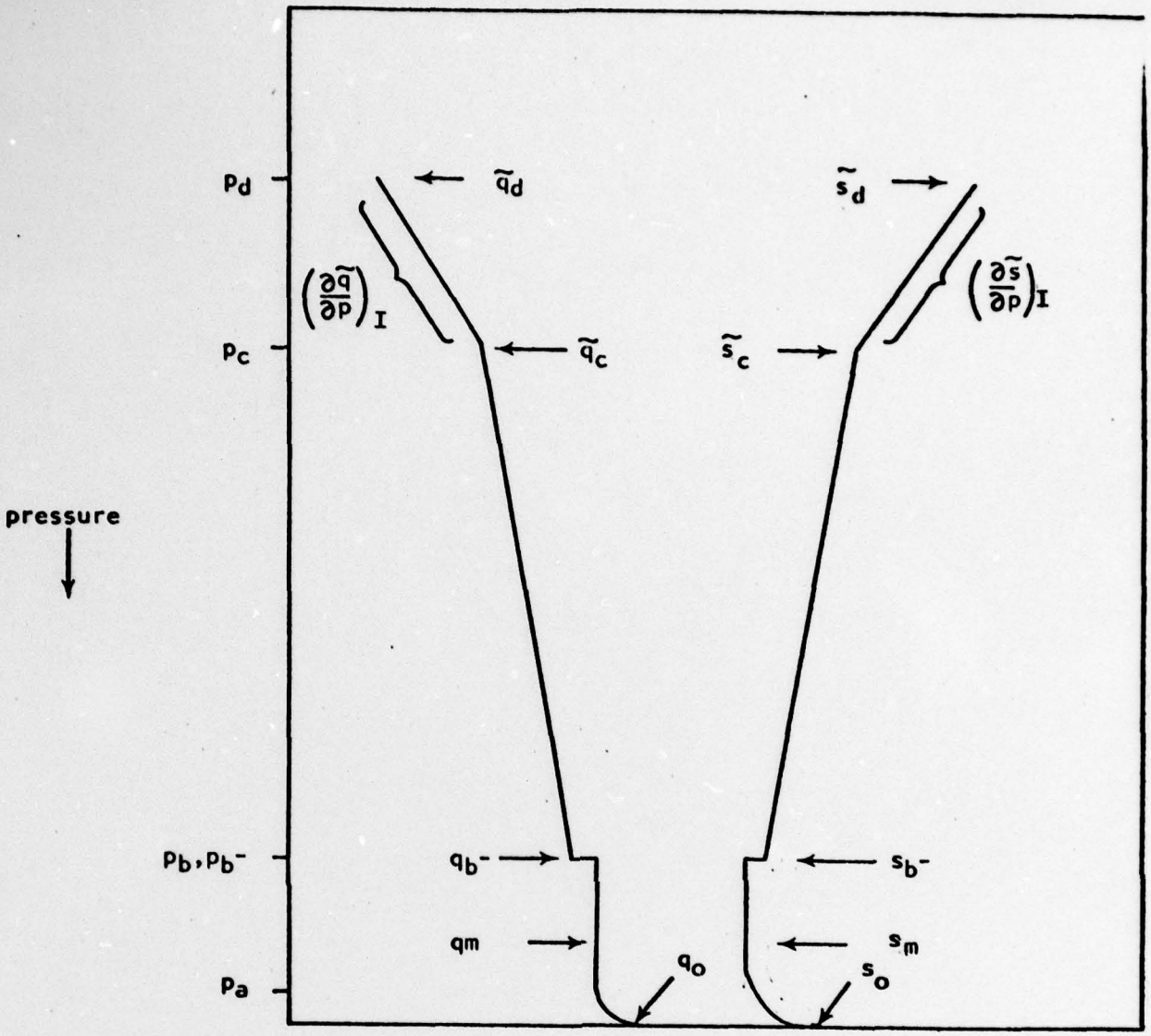

Figure 2. Assumed model profiles of $\tilde{s}$ and $\tilde{q}$. The values of p_d, $\tilde{s}_d$, $\tilde{q}_d$, $\left(\frac{\partial \tilde{s}}{\partial p}\right)_I$, and $\left(\frac{\partial \tilde{q}}{\partial p}\right)_I$ are imposed. All other quantities labeled on the figure are predicted by the coupled model.

$$1/2\,\frac{\partial p_c}{\partial t}\left[\tilde{s}_d - \tilde{s}_{b^-} + \left(\frac{\partial \tilde{s}}{\partial p}\right)_I (p_b - p_d)\right]$$

$$+\ 1/2\,\frac{\partial p_b}{\partial t}\left[\tilde{s}_d - \tilde{s}_{b^-} + \left(\frac{\partial \tilde{s}}{\partial p}\right)_I (p_c - p_d)\right] + 1/2\,\frac{\partial \tilde{s}_{b^-}}{\partial t}(p_b - p_c) =$$

$$\int_{p_d}^{p_b}\left[-\tilde{\vec{v}}\cdot\widetilde{\nabla_p s} + L_v\tilde{Q}_c + \tilde{Q}_R\right]dp -$$

$$\left(\frac{\partial \tilde{s}}{\partial p}\right)_I\int_{p_d}^{p_c}\tilde{\omega}dp - \frac{(\tilde{s}_{b^-} - \tilde{s}_c)}{(p_b - p_c)}\int_{p_c}^{p_b}\tilde{\omega}dp + \widetilde{(\omega' s')}_d - \widetilde{(\omega' s')}_{b^-} \qquad (81)$$

$$1/2\,\frac{\partial p_c}{\partial t}\left[\tilde{q}_d - \tilde{q}_{b^-} + \left(\frac{\partial \tilde{q}}{\partial p}\right)_I (p_b - p_d)\right] +$$

$$1/2\,\frac{\partial p_b}{\partial t}\left[\tilde{q}_d - \tilde{q}_{b^-} + \left(\frac{\partial \tilde{q}}{\partial p}\right)_I (p_c - p_d)\right] + 1/2\,\frac{\partial \tilde{q}_{b^-}}{\partial t}(p_b - p_c) =$$

$$\int_{p_d}^{p_b}\left[-\tilde{\vec{v}}\cdot\widetilde{\nabla_p q} - \tilde{Q}_c\right]dp - \left(\frac{\partial \tilde{q}}{\partial p}\right)_I\int_{p_c}^{p_c}\tilde{\omega}dp -$$

$$\frac{(\tilde{q}_{b^-} - \tilde{q}_c)}{(p_b - p_c)}\int_{p_c}^{p_b}\tilde{\omega}dp + \widetilde{(\omega' q')}_d - \widetilde{(\omega' q')}_{b^-} \qquad (82)$$

The rate of condensation minus evaporation, $\tilde{Q}_c$, can be eliminated between (81) and (82) to yield a prediction equation for p_c in terms of the large-scale forcing functions ($\tilde{\vec{v}} \cdot \tilde{\nabla} s$, $\tilde{\vec{v}} \cdot \tilde{\nabla} q$, $\tilde{\omega}$, $\tilde{Q}_R$ provided that $\partial s_{b^-}/\partial t$, $\partial q_{b^-}/\partial t$, $(\widetilde{\omega' s'})_{b^-}$, $(\widetilde{\omega' q'})_{b^-}$, $(\widetilde{\omega' s'})_d$, and $(\widetilde{\omega' q'})_d$ can be determined. This will close the model.

Following Betts (1976), prediction equations for $\tilde{s}_{b^-}$ and $\tilde{q}_{b^-}$ can be written

$$\frac{\partial \tilde{s}_{b^-}}{\partial t} = -(\tilde{\vec{v}} \cdot \widetilde{\nabla_p s})_b - (\tilde{\omega}_b - \omega_b^* - \frac{\partial p_b}{\partial t}) \frac{(\tilde{s}_c - \tilde{s}_{b^-})}{(p_c - p_b)}$$

$$+ (\tilde{Q}_R)_{b^-} + (\frac{\partial \omega^*}{\partial p})_b \Delta s \qquad (83)$$

$$\frac{\partial \tilde{q}_{b^-}}{\partial t} = -(\tilde{\vec{v}} \cdot \widetilde{\nabla_p q})_b - (\tilde{\omega}_b - \omega_b^* - \frac{\partial p_b}{\partial t}) \frac{(\tilde{q}_c - \tilde{q}_{b^-})}{(p_c - p_b)}$$

$$+ (\frac{\partial \omega^*}{\partial p})_b \Delta q \qquad (84)$$

where we have made use of (79) and assumed that the cloud updrafts at p_b have the mixed layer values of s and q. We have also assumed that cloud base occurs just above p_b and neglected the evaporation of any falling raindrops there. Consequently, there are no condensation or evaporation terms in (83) and (84).

The last terms on the right-hand-side of (83) and (84) represent important cooling and moistening effects, respectively, due to detrainment of cloud mass at p_b ($\partial\omega^*/\partial p < 0$). The diagnostic studies of Betts (1975) and Nitta (1975) have shown that the detrainment at $p_{\bar{b}}$ is large. We will parameterize it according to

$$\left(\frac{\partial \omega^*}{\partial p}\right)_b = k_1 \frac{\omega_b^*}{p_b - p_c} \tag{85}$$

where k_1 is a dimensionless constant. The BOMEX Phase III data analyzed by Nitta (1975) suggest $k_1 \cong 3$.

The eddy fluxes at $p_{\bar{b}}$ and above are assumed to be due solely to the presence of cumulus clouds which begin as updrafts with the thermodynamic characteristics of the mixed layer. Thus, again invoking the assumption that $\sigma << 1$, the eddy fluxes of dry static energy and moisture at $p_{\bar{b}}$ can be written (see Arakawa and Schubert, 1974)

$$(\widetilde{\omega' s'})_{b^-} = -\omega_b^* \Delta s$$

$$(\widetilde{\omega' q'})_{b^-} = -\omega_b^* \Delta q \qquad (86)$$

The diagnostic study of Nitta (1975) indicates that essentially all of the cumulus convection is confined to below the top of the trade inversion for typical undisturbed conditions. Hence, to good approximation we can write.

$$(\widetilde{\omega' s'})_d = 0$$

$$(\widetilde{\omega' q'})_d = 0 \qquad (87)$$

We now turn our attention to the convective vertical p-velocity at the top of the mixed layer, ω_b^*. In the spectral model of Arakawa and Schubert (1974), in which cloud types are differentiated from one another by their entrainment rates, ω_b^* is given by

$$\omega_b^* = -g \int_0^{\lambda max} m_b(\lambda)\, d\lambda \qquad (88)$$

where $m_b(\lambda)d\lambda$ is the cloud-induced vertical mass flux at p_b due to all the clouds in the ensemble with an entrainment rate of λ, and λ_{max} is the maximum entrainment rate for the ensemble. To calculate $m_b(\lambda)$ they introduce the "cloud work function," $A(\lambda)$, which is an integral measure of the buoyancy force for type λ clouds, and demonstrate that a cumulus ensemble will follow a sequence of quasi-equilibria with the large-scale atmospheric forcing. This implies

$$\frac{dA(\lambda)}{dt} = \int_0^{\lambda max} K(\lambda,\lambda')\, m_b(\lambda')d\lambda' + F(\lambda) = 0 \qquad (89)$$

which is a Fredholm integral equation that can be solved for $m_b(\lambda)$ since the kernel, $K(\lambda,\lambda')$, and the large-scale forcing, $F(\lambda)$, can be calculated from the large-scale fields alone.

The kernel gives the rate at which type λ' clouds stabilize the environment for type λ clouds per unit cloud mass flux through release of the moist convective instability. The dominant effect represented by $K(\lambda,\lambda')$ is adiabatic warming of the cloud layer due to cloud-induced subsidence in the environment. The large-scale forcing gives the rate at which large-scale processes destabilize the environment for type λ clouds. The dominant effects represented by $F(\lambda)$ in the undisturbed trades are radiative cooling in the cloud layer and heat and moisture convergence in the atmospheric mixed layer.

For the problem we consider in this paper, the actual form of the spectral distribution of the cumulus clouds is not of primary concern. Instead, we require only ω_b^* which is an integral over all the various cloud types. Thus, rather than determining the spectral distribution of the cloud mass flux from the full Arakawa-Schubert theory, we will use some ideas from it to parameterize ω_b^* in a very simple fashion. In particular, we write a simplified version of (89) as

$$K_A \int_0^{\lambda max} m_b(\lambda')d\lambda' + k_2 F_A = 0 \qquad (90)$$

where K_A and F_A are some characteristic values of the kernal and large-scale forcing respectively and k_2 is a proportionality constant.

We will take K_A to be the dominant term in the kernal for non-entraining (i.e. $\lambda = 0$) clouds which implies

$$K_A = \frac{g}{(p_b - p_c)} \int_{p_c}^{p_b} \frac{\partial \tilde{s}}{\partial p} \, dp \qquad (91)$$

where, for convenience, the average level of detrainment has been taken to be at p_c. Similarly, we write F_A as

$$F_A = F_C + F_M \qquad (92)$$

where F_C and F_M are characteristic cloud layer forcing and mixed layer forcing terms respectively. We take F_C to be the cloud layer forcing term from the original theory for non-entraining clouds, which yields

$$F_C = \frac{-R}{c_p} \int_{p_c}^{p_b} \left(-\tilde{\vec{v}} \cdot \widetilde{\nabla_p s} - \tilde{\omega}\frac{\partial \tilde{s}}{\partial p} + \tilde{Q}_R\right) \frac{dp}{p} \qquad (93)$$

We take F_M to be

$$F_M = \frac{R}{3c_p} \left(\frac{\partial s_m}{\partial t} + L_v \frac{\partial q_m}{\partial t}\right) \int_{p_c}^{p_b} \frac{dp}{p} \qquad (94)$$

which is motivated by the term arising from mixed-layer convergence of moist static energy in the original theory. Hence, using (79), (88), and (90) - (94), the convective vertical p-velocity at p_b can be written

$$\omega_b^* = k_2 \frac{R}{c_p} \frac{(p_b - p_c)}{(\bar{s}_{b-} - \bar{s}_c)} \left[1/3\left(\frac{\partial s_m}{\partial t} + L_v \frac{\partial q_m}{\partial t}\right) \int_{p_c}^{p_b} \frac{dp}{p} - \right.$$

$$\left. \int_{p_c}^{p_b} \left(-\tilde{\vec{v}} \cdot \widetilde{\nabla_p s} + \tilde{Q}_R\right) \frac{dp}{p} - \frac{(\tilde{\bar{s}}_{b-} - \tilde{\bar{s}}_c)}{(p_b - p_c)} \int_{p_c}^{p_b} \tilde{\omega} \frac{dp}{p}\right] \qquad (95)$$

A simplified conservation equation for liquid water (i.e. cloud droplets) can be written

$$\frac{\partial \bar{W}}{\partial t} = \frac{1}{(p_b - p_d)} \int_{p_d}^{p_b} \bar{Q}_c \, dp - P_o \qquad (96)$$

where $\bar{W}$ is defined by

$$\bar{W} = \sum_{i=1}^{N} W_i C_i \qquad (97)$$

with W_i the average liquid water mixing ratio (mass of liquid water per mass of air) of the ith cloud, C_i the fraction of the model domain covered by the ith cloud, and N the total number of clouds.

The first term on the right-hand-side of (96) can be determined from (81) and (82) and the precipitation rate can be parameterized according to

$$P_o = \frac{-k_3 \omega_b^* \bar{W}}{(p_b - p_c)} \qquad (98)$$

with k_3 a dimensionless proportionality constant. Thus, (96) can be used to predict $\tilde{W}$, from which an estimate of fractional cloud cover can be obtained by

$$C = \frac{\tilde{W}}{W_A} \tag{99}$$

where W_A is a characteristic value of liquid water mixing ratio for a typical cloud in the ensemble. Note that the contribution to C of any clouds other than those originating as updrafts from the mixed layer are ignored. Note also that σ may be much less than C since only a relatively small fraction of the existing cloud mass may be characterized by active updrafts.

Finally, we note that no attempt will be made to model the momentum profile in the cloud layer and above. Rather, the horizontal wind velocity vector will be imposed at p_b as an upper boundary condition for momentum.

Section 3
DESCRIPTION OF THE EXPERIMENTS

Two separate one-dimensional air-sea models, denoted by "D" and "B" are considered. The oceanic component of D is the diffusive model of Section 2.1.1, while for B it is the bulk model of Section 2.1.2. The atmospheric component of both models is described in Section 2.2.

The model equations (8) - (10), (20) - (22), (68) - (70), (81) - (84), and (96) are solved using forward time differencing with the diffusive terms treated implicitly. In B, a convective adjustment scheme that conserves heat, salinity, and momentum is employed to deepen the mixed layer in the event that the change in buoyancy across the entrainment zone (Δb) becomes negative. For both D and B, a uniform grid with spacing 1 m extends from the sea surface to a depth of 30.5 m. A vertical grid is not required for the model atmosphere.

Values used for the empirical constants needed in the diffusive oceanic model are those given by Mellor and Yamada (1974). Values used for the empirical constants required by the bulk oceanic model are those given by Garwood (1977) plus $p_3 = 30$ (see Garwood, 1977). All other constants can be found either in standard reference books or Table 1.

Table 1
Model Constants and Boundary Conditions

Quantity	Symbol	Value
Damping coefficient for inertial oscillations	D	7.5×10^{-6} s^{-1}
Coriolis parameter	f	3.77×10^{-5} s^{-1}
Empirical proportionality constants for model atmosphere	k_1, k_3, k_3	3,120,0.15
Average liquid water mixing ratio of clouds	W_A	2 gm kg^{-1}
Extinction coefficient for radiation in ocean	γ	0.09 m^{-1}
von Karman's constant	κ	0.4
Temperature at bottom of ocean models	T_B	28.025°C
Salinity at bottom of ocean models	S_B	34.09 o/oo
Wind velocity vector at top of transition layer	$(\underset{\rightarrow}{v})_b$	$-10\ \hat{i}$ m s^{-1}
Dry static energy at top of trade inversion	$\tilde{s}_d$	3.040×10^{-5} j kg^{-1}
Water vapor mixing ratio at top of trade inversion	$\tilde{q}_d$	5 gm kg^{-1}

We simulate Phase III Period A of BOMEX (21 - 26 June 1969) by adopting values of the imposed large-scale forcing functions that are based on observations during this period. Table 2 summarizes the forcing functions for all experiments reported here. Note that, following Pandolfo and Jacobs (1972), the large-scale vertical motion in the atmosphere and the horizontal advections will be taken as time invariant in the experiments. The forcing terms due to radiational heating of the atmosphere, however, are allowed to vary diurnally to account for direct absorption of solar radiation by the air. The amplitude of the heating rate is in accordance with climatological estimates and the time-averaged heating rate is in close agreement with the values reported for the BOMEX area by Nitta and Esbensen (1974). Note also that the time-averaged solar flux penetrating the sea surface for all experiments is within 1 - 2 ly day^{-1} of the value observed at the research vessel Discoverer (13° 08' N, 53° 51'W) during the period in question.

We mention here that Nitta and Esbensen (1974) observed a diurnal fluctuation in large-scale vertical motion over the BOMEX area which they attributed to the land sea contrast. However, its contribution to the diurnal heating rate of the atmosphere below the trade inversion is small compared to the diurnal variation in radiative heating and it may be confined only to the coastal regions anyway. Therefore, it is neglected here.

The initial profiles of temperature and salinity in the upper ocean are the same for all experiments and given by observations at Discover. The initial velocity profile in the upper ocean for all experiments is taken to be independent of depth and given by $\vec{v} = (-0.08\,\hat{i} + 0.21\hat{j})$m s^{-1}.

Table 2

IMPOSED LARGE-SCALE FORCING FUNCTIONS

Quantity	Symbol	Assumed Values
Lateral advection of temperature in ocean	$\bar{\vec{v}} \cdot \nabla\bar{T}$	From Delnore (1972)
Lateral advection of salinity	$\bar{\vec{v}} \cdot \nabla\bar{S}$	0
*Solar flux penetrating sea surface in the absence of clouds	F_i	$\begin{cases} 1165 \left\{ \sin \left[\frac{(LST-0900)\pi}{0600} \right] + 1 \right\} ly\ day^{-1} & \text{for } 0600 \leq LST \leq 1800 \\ 0 \text{ otherwise} \end{cases}$
Net radiational heating rate of air averaged between the surface and the top of the mixed layer	$(\tilde{Q}_R)_{ab}$	$\begin{cases} \left\{ -2.5 + 1.2 \left\{ \sin \left[\frac{(LST-0900)\pi}{0600} \right] + 1 \right\} \right\} c_p \ ^{o}C\ day^{-1} \\ \text{for } 0600 \leq LST \leq 1800 \\ -2.5\, c_p \ ^{o}C\ day^{-1} \quad \text{otherwise} \end{cases}$
Net radiational heating rate of air at top of transition layer	$(\tilde{Q}_R)_{b^-}$	$(\tilde{Q}_R)_{ab}$
Net radiational heating rate of air averaged between the top of the transition layer and the top of the trade inversion	$\frac{\int_{p_d}^{p_b} \bar{Q}_R \, dp}{(p_b - p_d)}$	$\begin{cases} \left\{ -1.6 + 1.2 \left\{ \sin \left[\frac{(LST-0900)\pi}{0600} \right] + 1 \right\} \right\} c_p \ ^{o}C\ day^{-1} \\ \text{for } 0600 \leq LST \leq 1800 \\ -1.6\, c_p \ ^{o}C\ day^{-1} \quad \text{otherwise} \end{cases}$

(Continued on following page)

Table 2 (Continued)

IMPOSED LARGE-SCALE FORCING FUNCTIONS

Quantity	Symbol	Assumed Values
Large-scale vertical p-velocity	$\tilde{\omega}$	From Soong and Ogura (1976)
Lateral advection of dry static energy	$\tilde{v} \cdot \overline{\nabla s}$	From Soong and Ogura (1976)
Lateral advection of water vapor mixing ratio	$\tilde{\mathbf{V}} \cdot \overline{\nabla q}$	From Soong and Ogura (1976)
Mixed-layer averaged geostrophic wind velocity vector	$(\tilde{\mathbf{V}}_g)_{ab}$	$(\tilde{\mathbf{V}}_g)_{ab} = -18\,\hat{i} + 0\hat{j}$ ms^{-1}
Lapse rate of dry static energy in the trade inversion	$\left(\frac{\partial \tilde{s}}{\partial p}\right)_I$	-1.18×10^{2} j kg^{-1} mb^{-1}
Lapse rate of water vapor mixing ratio in the trade inversion	$\left(\frac{\partial \tilde{q}}{\partial p}\right)_I$	6.81×10^{-2} gm kg^{-1} mb^{-1}

* LST ≡ Local Standard Time

The initial conditions for the atmosphere are the same for all experiments and are obtained by imposing the large-scale forcing functions in Table 2, holding the sea surface temperature fixed at its initial value, and integrating the model to a cyclical steady state from arbitrary initial conditions. Thus, the initial atmospheric state is in equilibirum with the large-scale atmospheric forcing and the sea surface temperature. The time invariant upper and lower boundary conditions for the coupled model are the same for all experiments and given in Table 1.

A total of four experiments are performed and the model configuration for each is summarized in Table 3. Experiments I and II are accomplished with the basic models described in Section 2. Experiment III is the same as I except that the sea surface temperature supplied to the model atmosphere is held constant at its initial value even though changes are predicted by the model ocean. Thus, the system is "half-coupled" since the model atmosphere is not allowed to "see" any changes in sea surface temperature predicted by the model ocean. Experiment IV is the same as I except that the radiational heating rate of the atmosphere $\tilde{Q}_R$ is held constant at its time-averaged value for Experiment I.

Table 3

SUMMARY OF EXPERIMENTS

Experiment	Model	Description
I	D	Basic model
II	B	Basic model
III	D	Half-coupled
IV	D	$\tilde{Q}_R$ held constant

Section 4
RESULTS

4.1 Mean Thermodynamic Structure of the Atmosphere and Mean Surface Fluxes

Fig. 3 shows vertical profiles of temperature and water vapor mixing ratio predicted by the model atmosphere averaged over the course of Experiment I. Also shown are horizontally-averaged observed vertical profiles of these quantities over the BOMEX area during the period in question. In general, agreement between the model predicted profiles and the observations below the base of the trade inversion is good, except for water vapor mixing ratio in the region between 950 and 975 mb. This is because the observations do not show a high degree of vertical uniformity for $\tilde{q}$ in the mixed layer. Deardorff (1978) has noted that differential horizontal advection of moisture (i.e. $\partial/\partial p(\tilde{\underline{v}}.\tilde{\nabla}q) \neq 0$) is quite capable of destroying the well-mixed structure of q over the tropical ocean, and this seems to be the case here.

Note, however, from Figure 3(a) that the well-mixed assumption for dry static energy seems to be good in this case since the observed and predicted temperature profiles are in extremely good agreement in the lowest 50 mb. The greater tendency toward vertical homogeneity for dry static energy has been explained by Deardorff (1978) in terms of a feedback between the intensity of the turbulence and the vertical gradient of dry static energy.

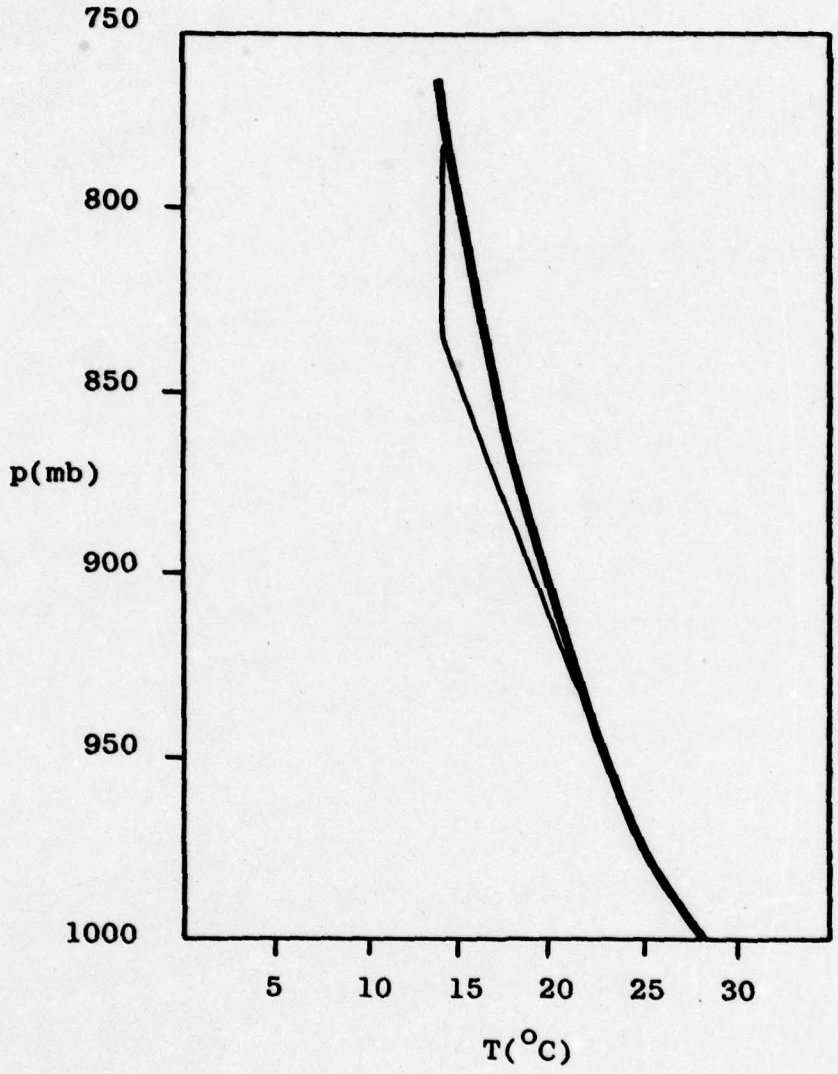

Figure 3(a). Mean temperature profile over the BOMEX area during the period 22-26 June (———) and mean temperature profile predicted for Experiment I (——).

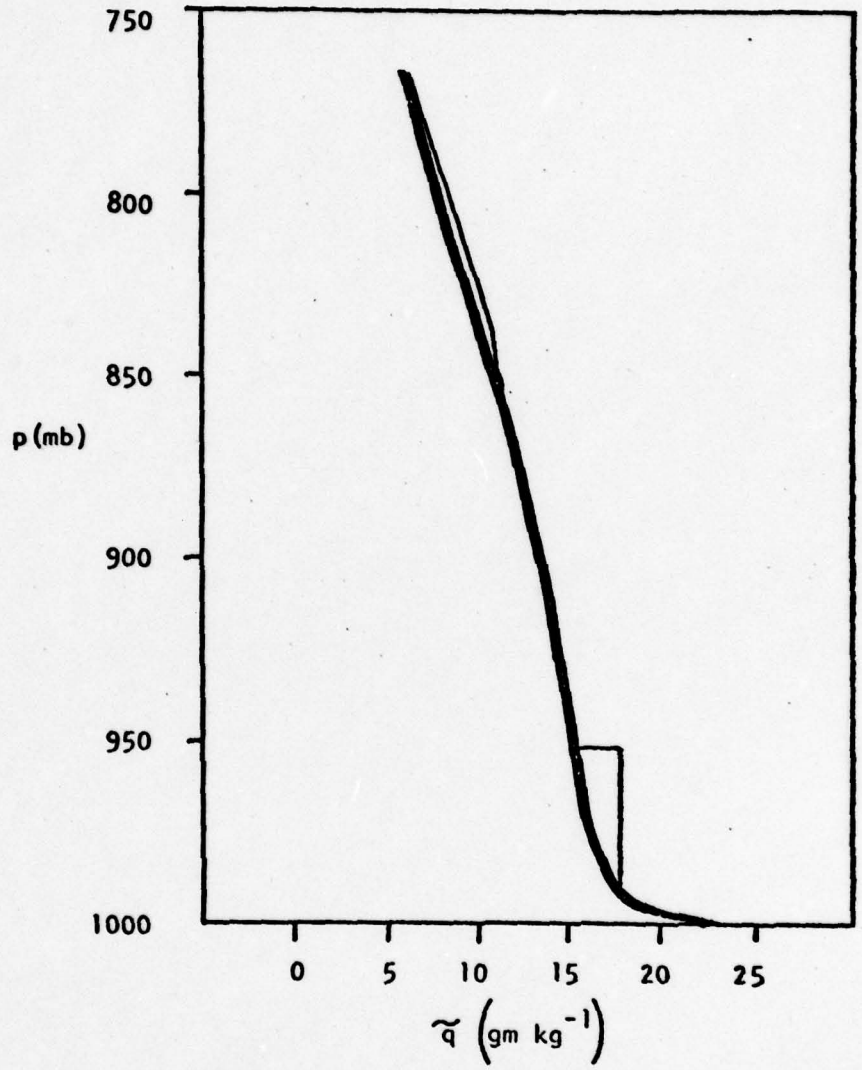

Figure 3(b). Mean water vapor mixing ratio profile over the BOMEX area during the period 22-26 June 1969 (▬▬) and mean water vapor mixing ratio profile predicted for Experiment I (——).

Because the model atmosphere does a good job of predicting the observed mean vertical structure of q and s, it is expected that the mean surface fluxes of sensible and latent heat are also well predicted. This expectation is confirmed by Table 4 which summarizes various estimates of $H_o + L_v Q_o$ in the BOMEX area during the period of interest. Note that the average of the estimates based on observations is 405 ly day^{-1}, while the value resulting from Experiment I is 415 ly day^{-1} which is good agreement. The value of 272 ly day^{-1} predicted by the coupled-model of Pandolfo and Jacobs (1972), however, appears anomalously small. This may be because all vertical eddy fluxes were parameterized using eddy diffusion coefficients in their model and no account was taken of moisture phase changes associated with cumulus clouds.

Table 4

Estimated Average Surface Sensible Plus
Latent Heat Flux in the BOMEX Area
for 22 - 26 June 1969

$H_o + L_vQ_o$ (ly day^{-1})	Source	Method
371	Delmore (1972)	oceanic heat budget
379	Holland and Rasmusson (1973)	atmospheric heat and moisture budget
420	Nitta and Esbensen (1974)	atmospheric heat and moisture budget
452	Nitta and Esbensen (1974)	bulk aerodynamic calculations
272	Pandolfo and Jacobs (1972)	coupled air-sea model integration
415	present study	coupled air-sea model integration (time average from Experiment I)

4.2 Diurnal Variability of the Upper Ocean and Comparison of Diffusive and Bulk Models of the Oceanic Mixed Layer

We will now compare the diurnal response of the diffusive and bulk models of the upper ocean. Fig. 4 shows time series of sea surface temperature predicted by Experiments I and II along with observations at Discoverer. Note here that, while the surface fluxes are not exactly the same for Experiments I and II because of the difference in predicted sea surface temperature, at no time does the net surface heat flux differ by more than 1% between the two experiments. Therefore, differences between the predicted oceanic fields of Experiments I and II are due almost entirely to intrinsic differences between the diffusive and bulk models.

Fig. 4 indicates that the phase of the predicted diurnal fluctuation in sea surface temperature is the same for both experiments, but the amplitude is larger for Experiment II. Furthermore, good agreement is found between the results of both experiments and the observations, although the amplitude of the fluctuation for Experiment I seems to be more realistic than that of Experiment II. Note also from Fig. 4 that the differences between the two model-predicted curves are largest in the afternoon when the sea surface temperature peaks but are very small near dawn when the sea surface temperature is at its minimum. To explain this difference between the response of the two models, we must examine the predicted internal structure of the upper ocean.

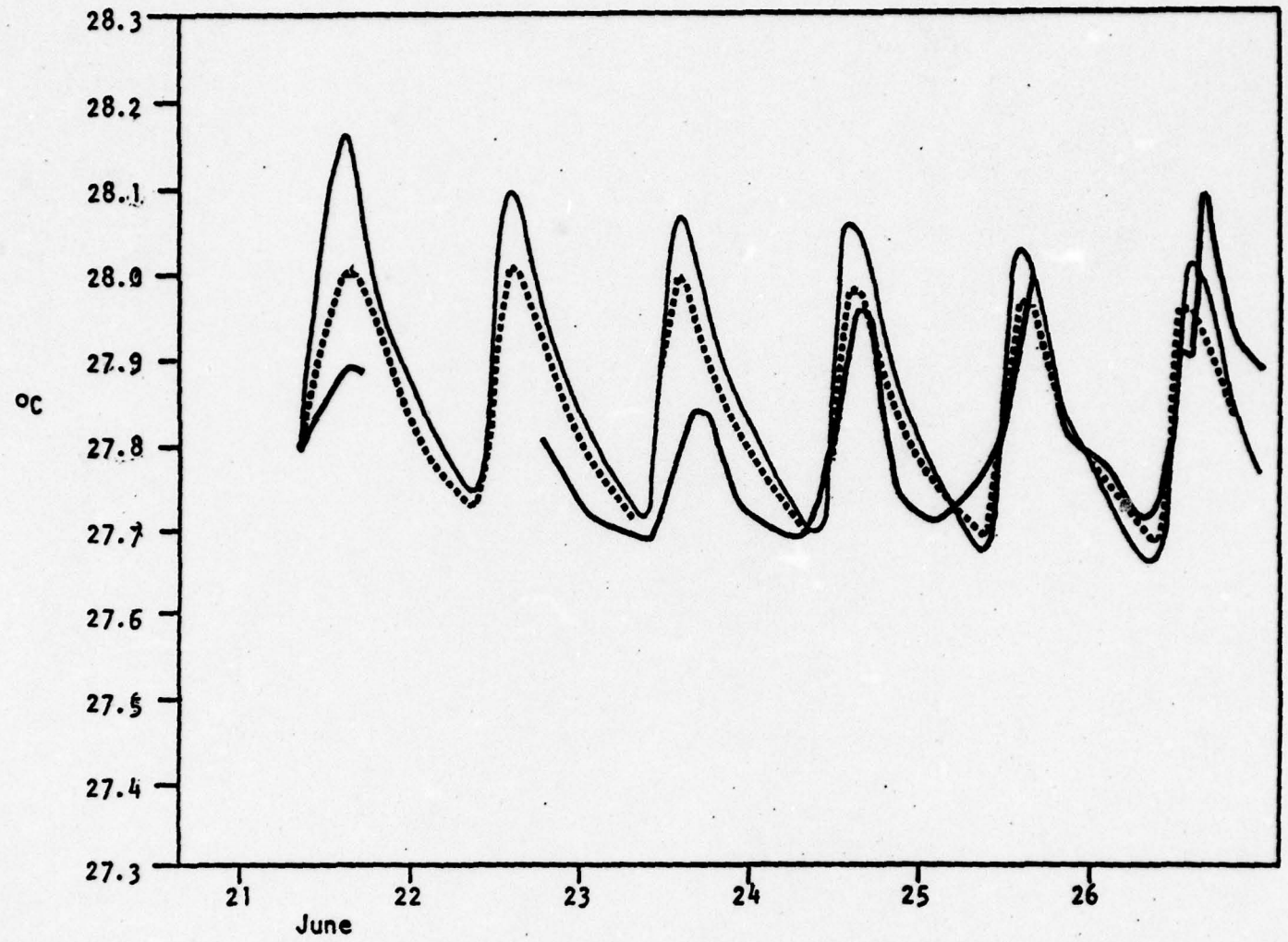

Figure 4. Six-day time series of (a) observed temperature at 6 m depth at Discoverer (———), (b) sea surface temperature predicted in Experiment I (- - - - - - - -), (c) sea surface temperature predicted in Experiment II (———).

Fig. 5 shows profiles of temperature in the upper 25 m of the ocean for both Experiments I and II at eight selected times during the day averaged over the five-day experimental period. Also shown are temperature profiles observed at Discoverer and averaged in the same way by Delnore (1972). Note that the horizontal arrow on each figure indicates the depth at which the turbulent kinetic energy predicted by model D goes to zero. Note also that the temperature increase with depth below the mixed layer is characteristic of the BOMEX area and does not represent an unstable stratification because of an associated salinity increase with depth in this region.

Fig. 5(a) shows the profiles at 0800 LST, two hours after sunrise, and the mixed layer is still near its maximum depth. Although the results of both models compare quite favorably to the observations, model B seems to do a better job of predicting both mixed layer depth and temperature.

Fig. 5(b) shows the profiles at 1100 LST and in this case both models show some difficulty in simulating the observed temperature structure. Moreover, at this point in the heating cycle fundamental differences in the two models begin to appear. For example, in model D turbulent mixing extends down to 15 m while model B predicts that all turbulence ceases below 7.5 m. In addition, heat supplied near the surface is diffused downward with some finite diffusive time scale in model D which results in a temperature

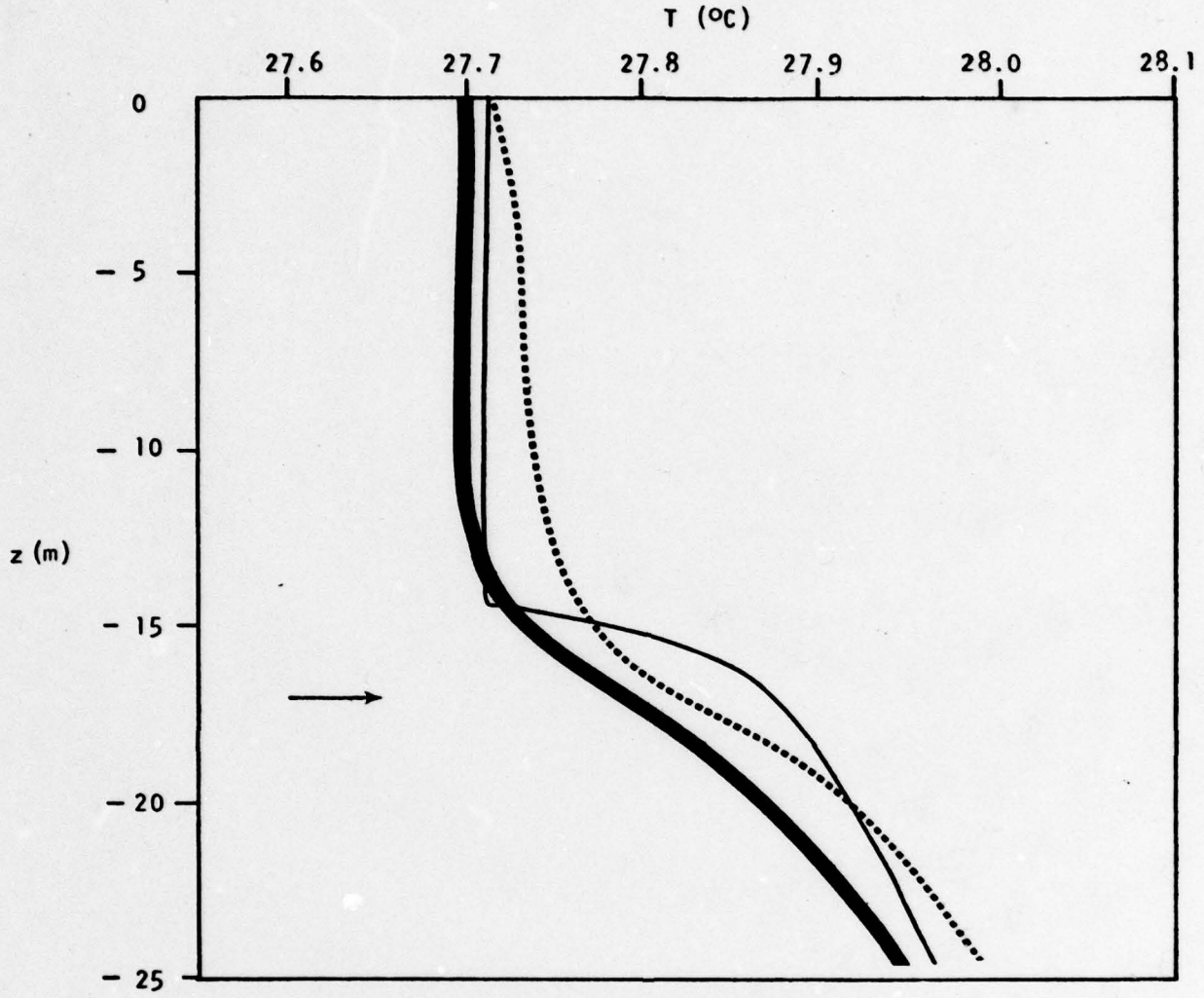

Figure 5(a). Vertical profiles of temperature in the upper ocean at 0800 LST averaged over the 6 day experimental period. Observations at Discoverer (▬▬▬), Experiment I (- - - - - - - -), Experiment II (————). The arrow indicates the depth at which turbulent kinetic energy predicted by model D goes to zero.

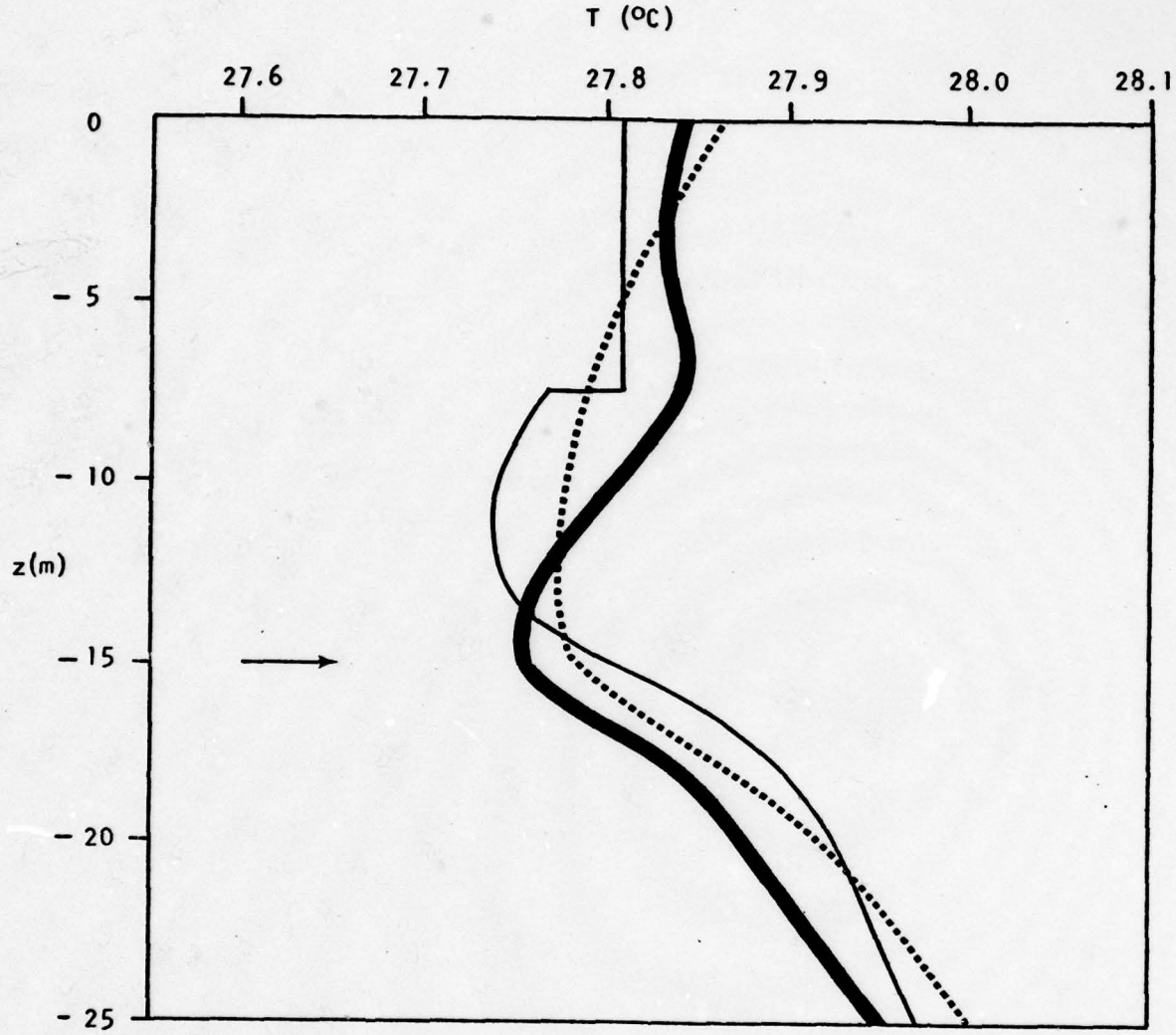

Figure 5 (b). Same as 5(a) but for 1100 LST.

decrease with depth near the surface. In model B, however, any heat added near the surface is instantaneously mixed throughout the mixed layer.

Fig. 5(c) shows the profiles at 1400 LST and here model D does a much better job of predicting the thermal structure than model B. Specifically, model B predicts a region of excessively warm water between the surface and 2.5 m depth and a region of excessively cool water between 7 and 15 m depth. This occurs because turbulent mixing near the time of maximum solar heating is confined to the upper few meters in model B so that heat supplied near the surface is absorbed in a relatively thin layer. Consequently, this thin layer becomes anomalously warm (hence the larger diurnal amplitude of sea surface temperature predicted by model B on Fig. 4) while the region below becomes anomalously cool. For model D, however, turbulent mixing still extends down to a depth of 15 m, which seems to be more realistic in view of the excellent agreement between the observations and the predicted profile for D. The rate at which model D diffuses heat downward during the day is also in fair agreement with the observations of the tropical diurnal thermocline made by Ostopoff and Worthem (1974).

In general, the mixed layer turbulent kinetic energy for bulk models changes instantaneously with the net surface heat flux. For most diffusive models, however, the net surface heat flux does not affect the turbulent kinetic energy throughout the mixed layer directly. Rather, it changes the turbulent kinetic energy indirectly through its effect on stratification, which is more physically realistic than the bulk model assumption. Furthermore, since the stratification is altered on some

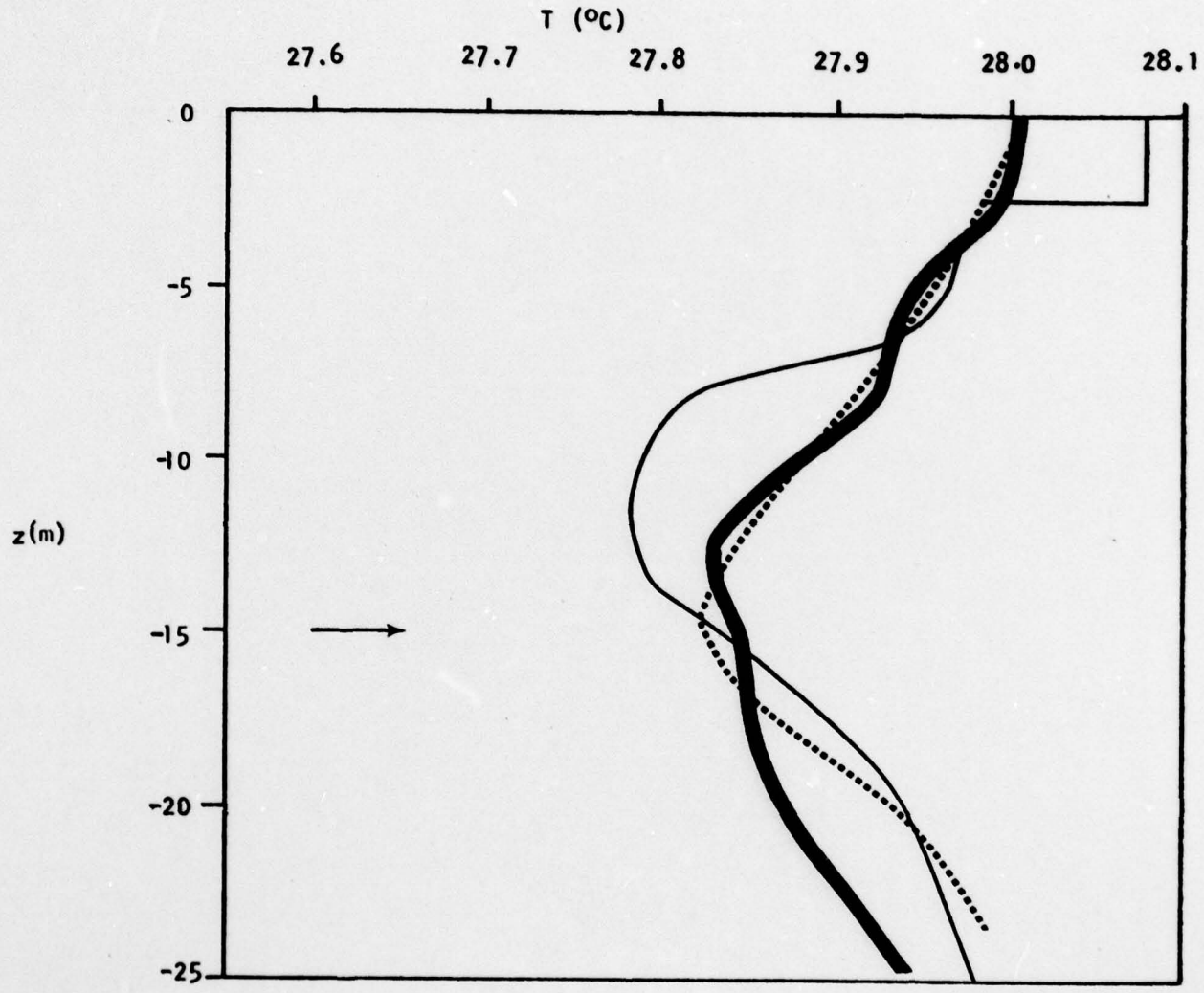

Figure 5(c). Same as 5(a) but for 1400 LST.

finite diffusive time scale in a diffusive model, the turbulent kinetic energy will lag the net surface heat flux. Thus, if the net surface heat flux changes substantially on a time scale that is not long compared to the diffusive time scale of the upper ocean, then the response of a diffusive model, because of its inherent adjustment time, is expected to be more realistic than that of a bulk model. This expectation seems to have been confirmed here.

Fig. 5(d) - 5(h) trace the thermal structure through the rest of the diurnal cycle. Note that discrepancies between the observations and the predicted profiles for both models D and B become progressively smaller with time during the night. In fact, the combined performance of the models seems to be best near dawn. This is because the net surface heat flux varies little with time during the night which, in contrast to the situation during the day, allows the upper ocean to approach an equilibrium state with the surface forcing.

4.3 Diurnal Variability of the Lower Atmosphere and Air-Sea Interaction

We now consider the way in which the diurnally varying solar radiative flux forces a diurnal response in the model atmosphere. The solar flux affects the atmosphere through two mechanisms: direct radiational heating of the air and direct radiational heating of the ocean. The second mechanism arises because the sea surface temperature provides the lower boundary conditions for temperature and humidity to the atmosphere. To examine the relative importance of

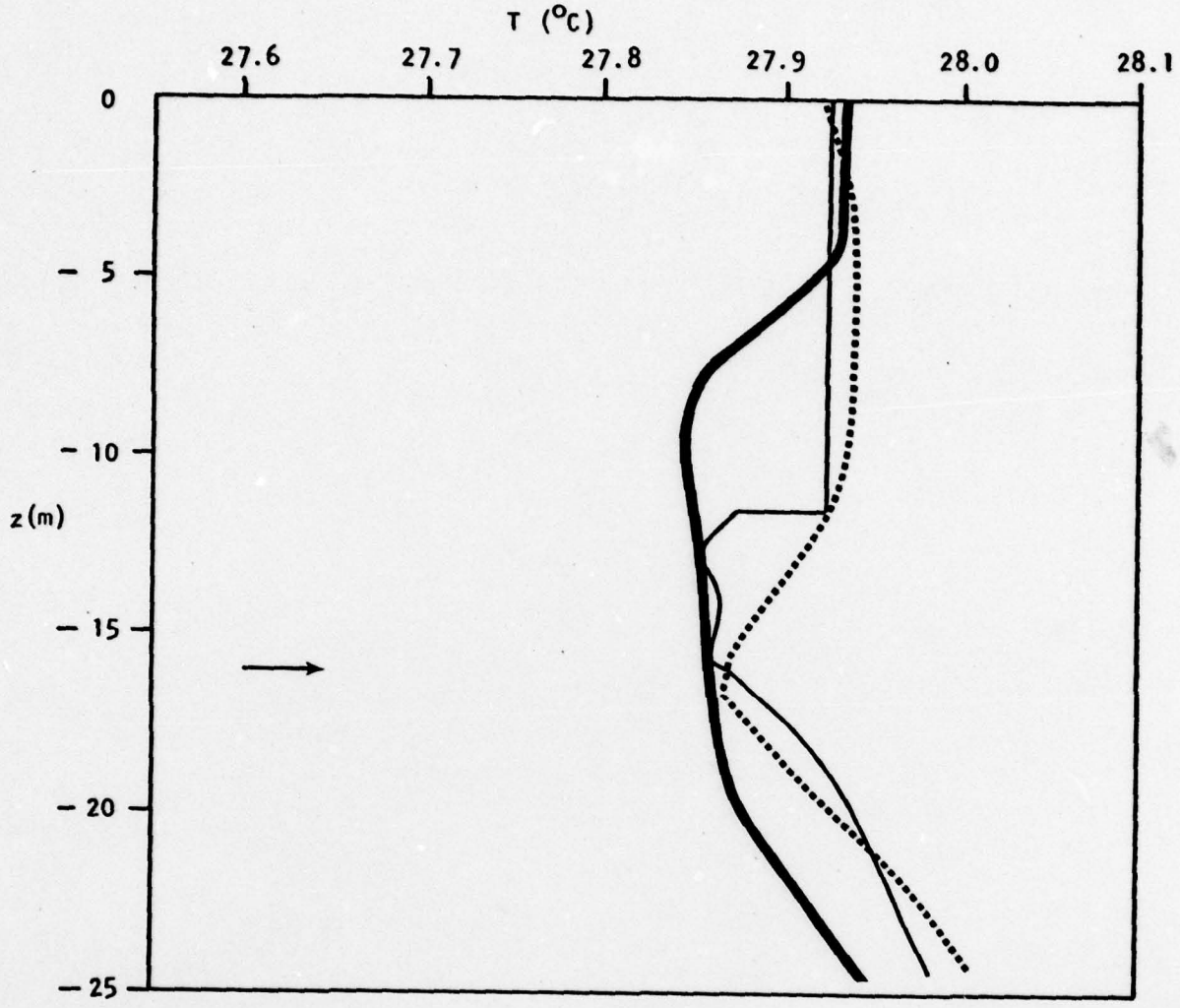

Figure 5(d). Same as 5(a) but for 1700 LST.

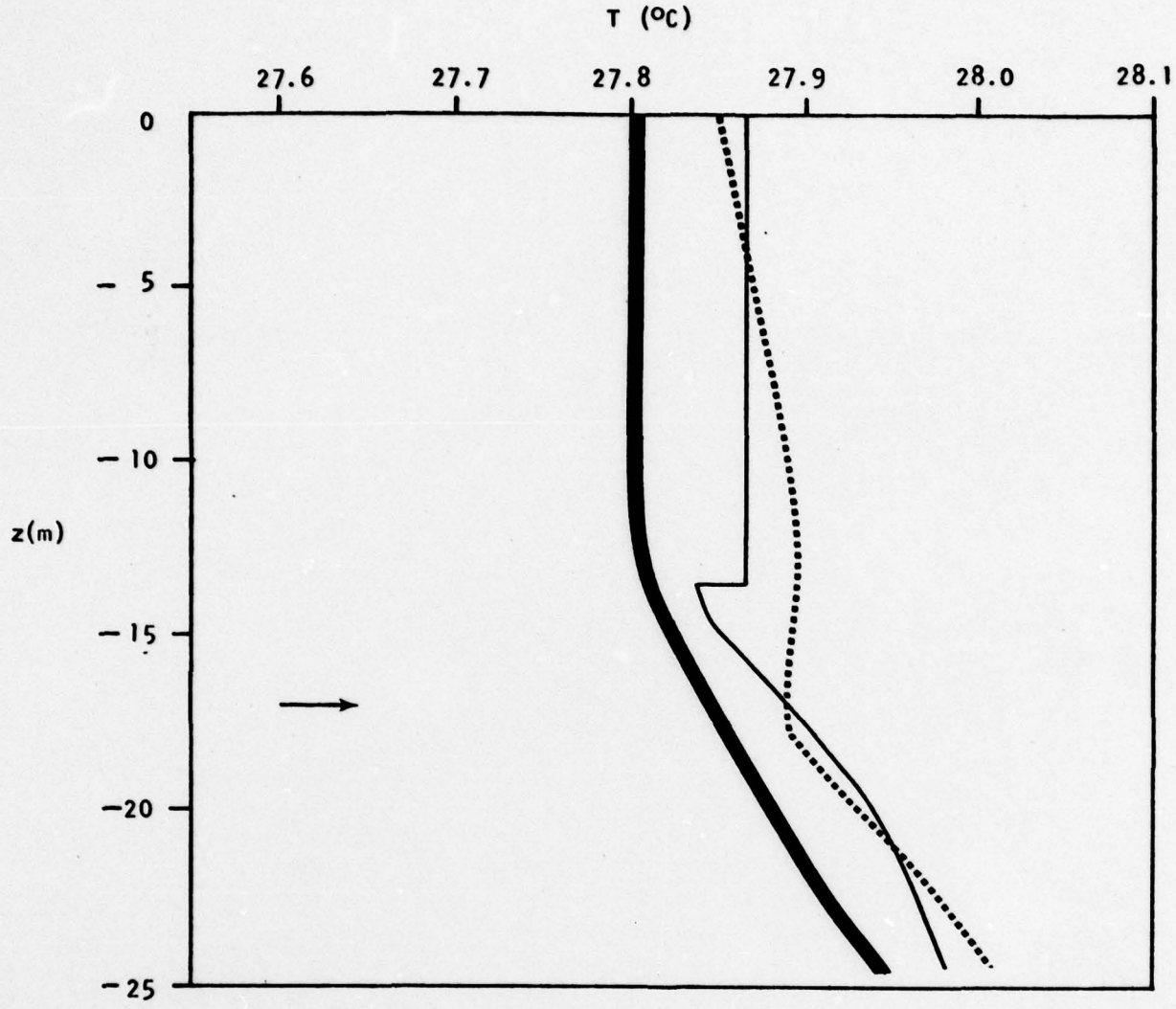

Figure 5(e). Same as 5(a) but for 2000 LST.

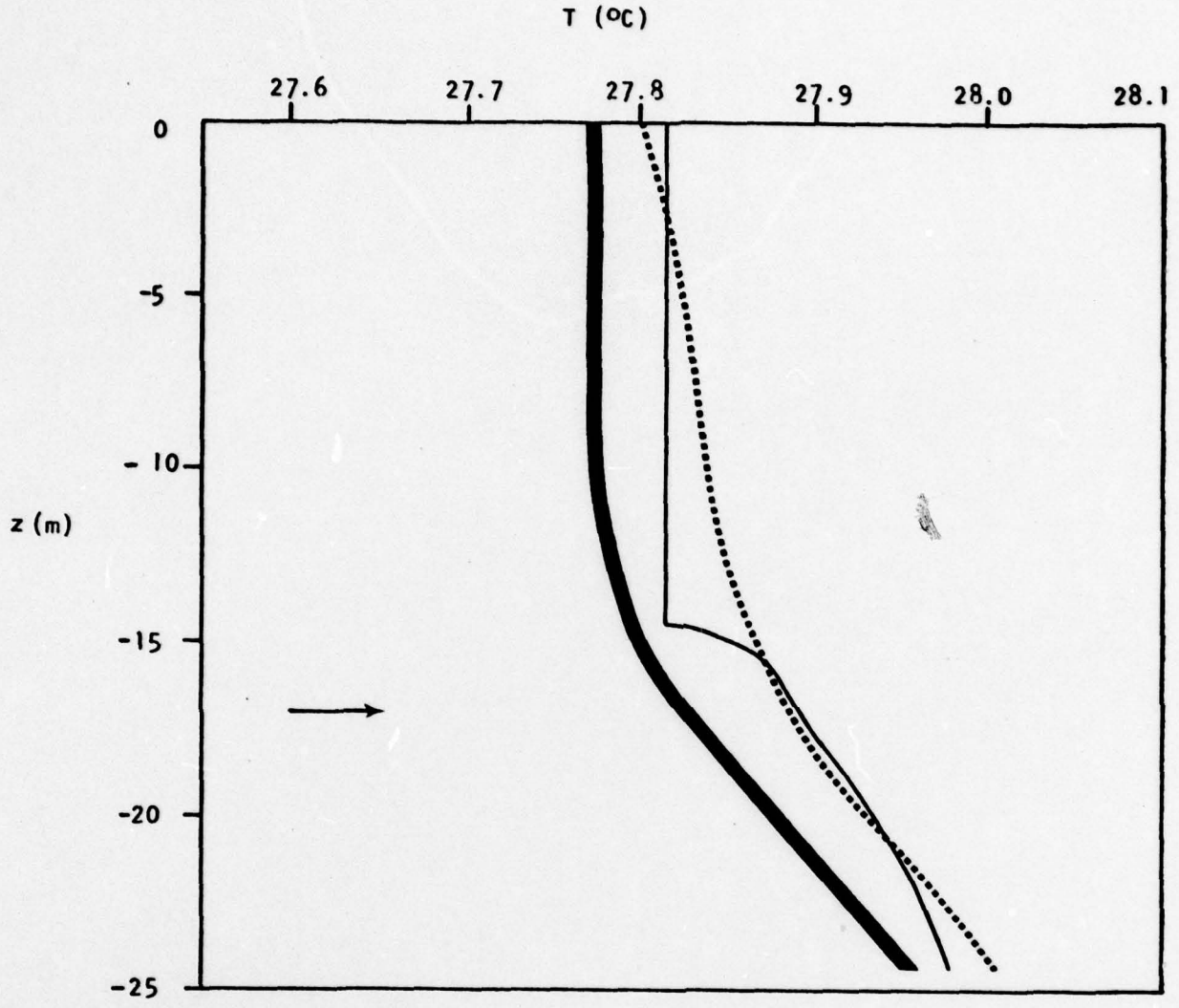

Figure 5(f). Same as 5(a) but for 2300 LST.

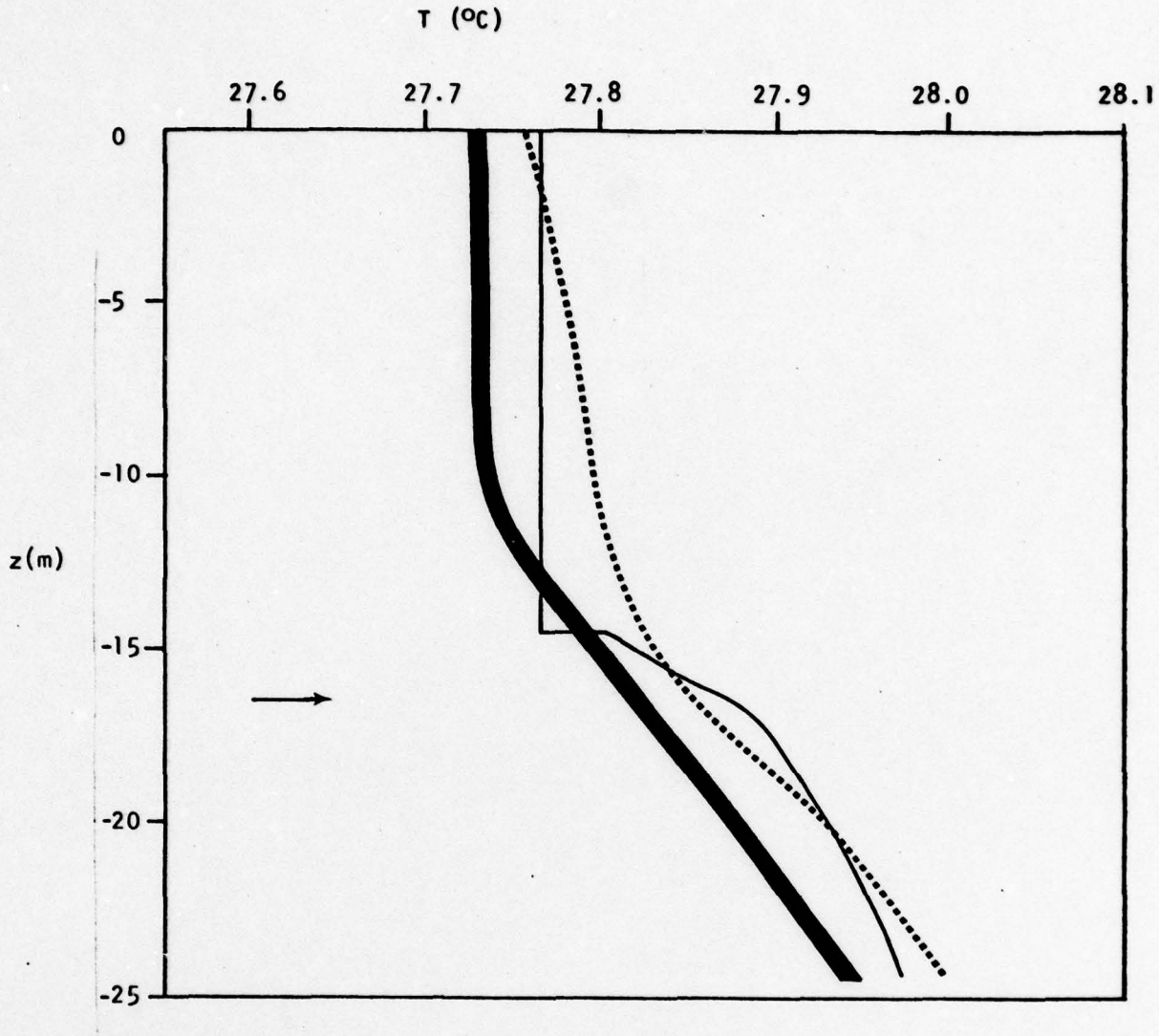

Figure 5(g). Same as 5(a) for 0200 LST.

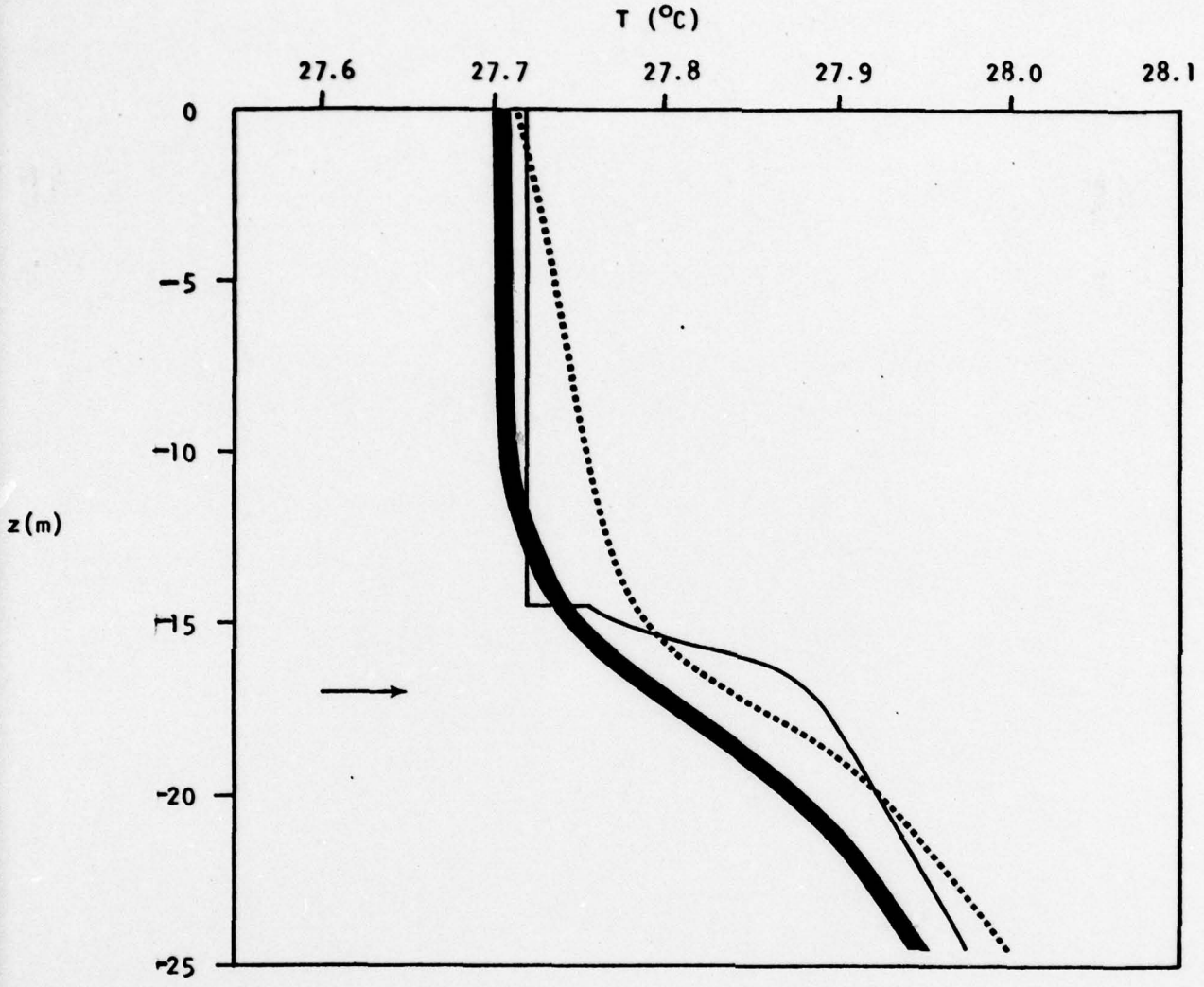

Figure 5(h). Same as 5(a) but for 0500 LST.

these forcing mechanisms and to investigate the possibility of feedback processes between the atmosphere and the ocean on the diurnal time scale, we will consider time series of various quantities predicted by the coupled-model on day 6 of Experiments I, III, and IV (see Table 3). Note that because the coupled-model response is nearly cyclical for all the experiments, the predicted fields on day 6 are characteristic of any day during the experimental period.

Fig. 6 shows time series of sea surface temperature on day 6 for Experiments I, III, and IV. The striking characteristic of this figure is that there is practically no difference between the three curves. Since in Experiment III the sea surface temperature supplied to the model atmosphere is held constant at its initial value, this implies that changes induced in the model atmosphere by these short time scale variations in sea surface temperature do not feed back significantly to the model ocean. Furthermore, since the radiational heating rate of the atmosphere is held constant at its time-averaged value in Experiment IV, Fig. 6 implies that diurnal fluctuations in direct radiational heating of the model atmosphere do not significantly affect the model ocean.

Fig. 7 shows time series of the convective vertical p-velocity at the top of the mixed layer ω_b^*. Note that ω_b^* takes on a maximum at night and a minimum during the day for both Experiments I and III, which is well known behavior for cumulus convection over the sea (Hann (1901), Lavoie (1963), Kraus (1963), Jacobson

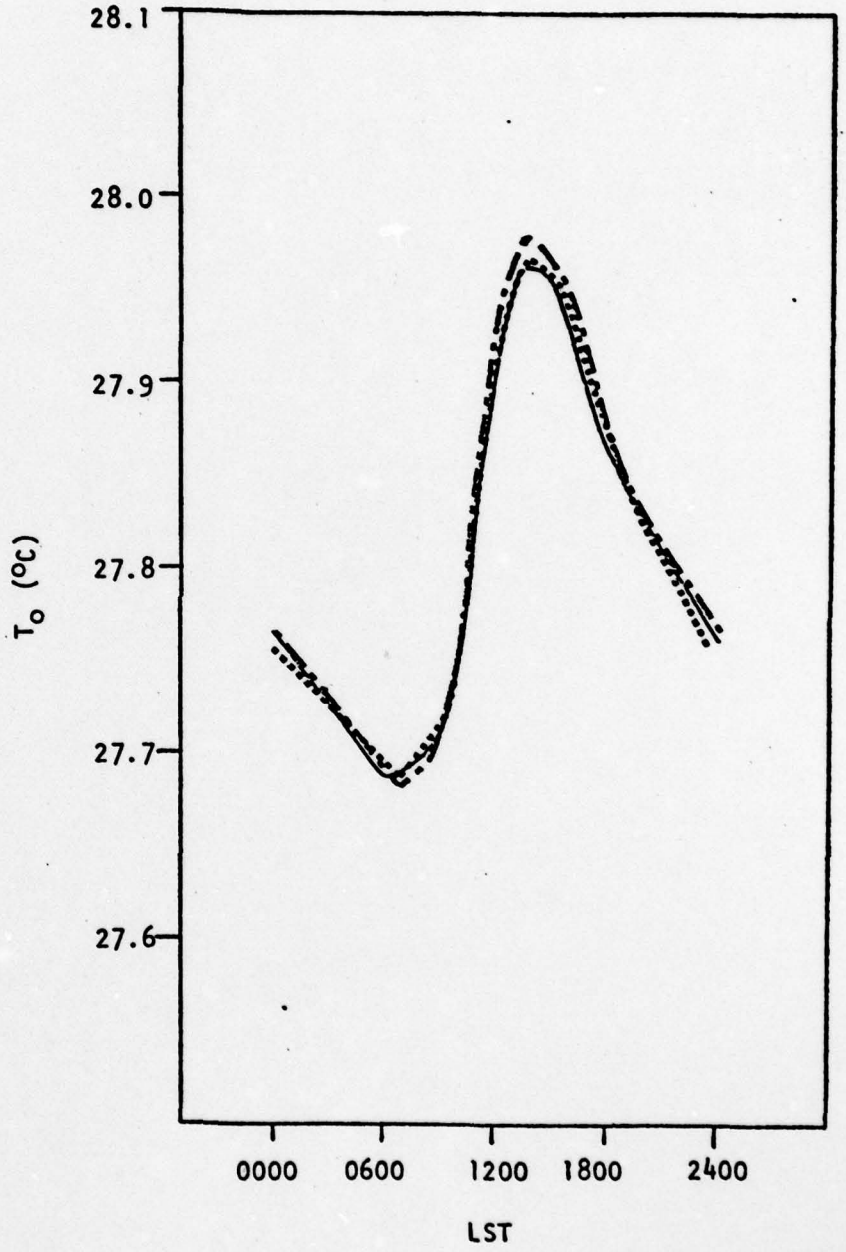

Figure 6. Time series of sea surface temperature on day 6 for Experiments I (———), III (·····), and IV (·—·—).

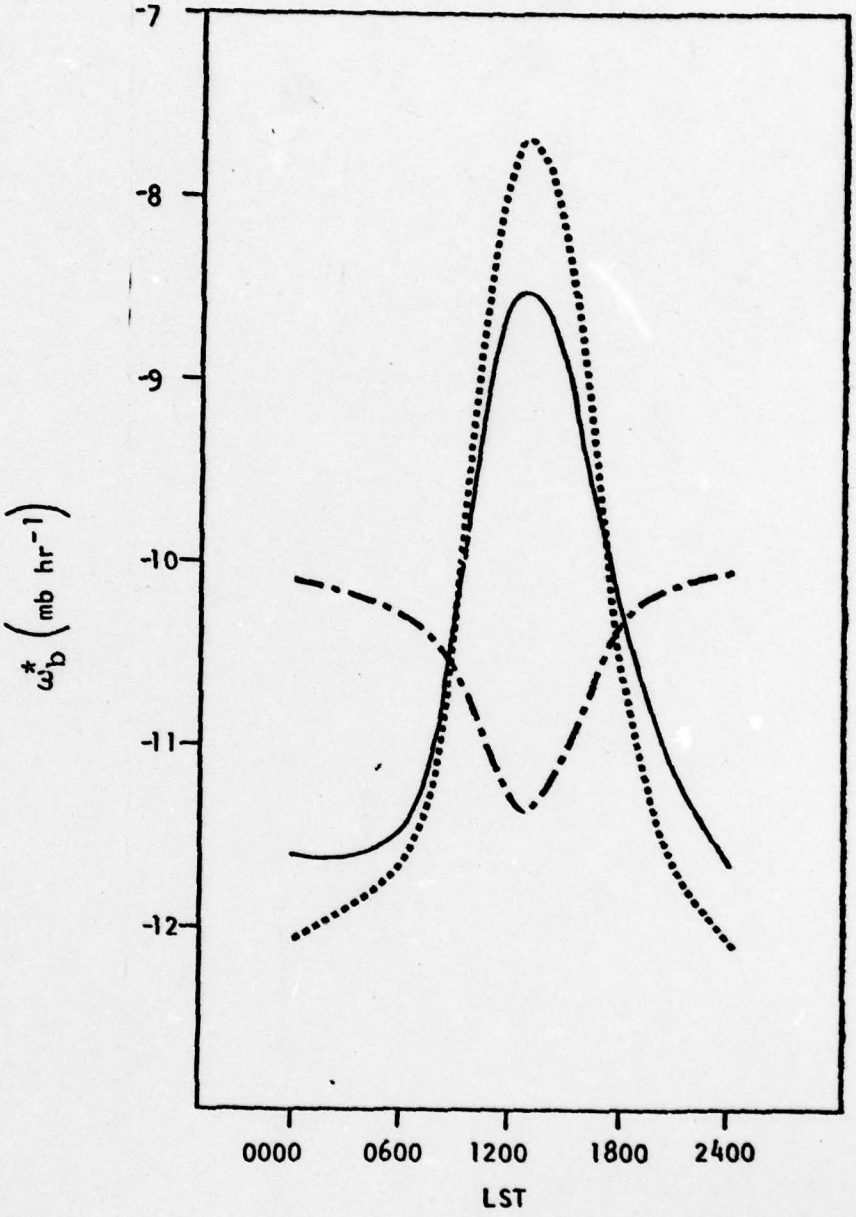

Figure 7. Time series of convective vertical p-velocity at top of atmospheric mixed layer on day 6 for Experiements I (———), III (-------), and IV (—·——).

(1976), Gray and Jacobson (1977)). Experiment IV, on the other hand, exhibits a much smaller diurnal variation for ω_b^* and is approximately 180° out of phase to the curves of Experiments I and III (see Fig. 7). Thus, since the sea surface temperature supplied to the model atmosphere is virtually the same for Experiments I and IV (see Fig. 6), this implies that the nighttime maximum and daytime minimum in cumulus convection in the model for Experiments I and II is due to radiational heating of the atmosphere. During the day, warming of the cloud layer by direct absorption of solar radiation tends to decrease the cloud layer forcing term (see Equation 93) and, as a result, the cloud activity weakens. At night, infrared cooling of the cloud layer has the opposite effect and the cumulus convection increases. This mechanism is similar to that proposed by Gray and Jacobson (1977).

Note also from Figure 7 that ω_b^* for Experiment I is larger during the day and smaller at night than ω_b^* for Experiment III. This is because warmer sea surface temperatures during the day tend to increase the cloud work function and enhance the cumulus convection, while the reverse is true at night (recall that the sea surface temperature supplied to the model atmosphere is held constant in Experiment III). Thus, the diurnal sea surface temperature fluctuation tends to suppress the diurnal variation in cumulus convection in the model.

Fig. 8 shows time series of fractional cloud coverage C. For both experiments I and III, the cloud coverage lags the convective vertical p-velocity by about 8 hours, thus taking on a maximum in the morning and a

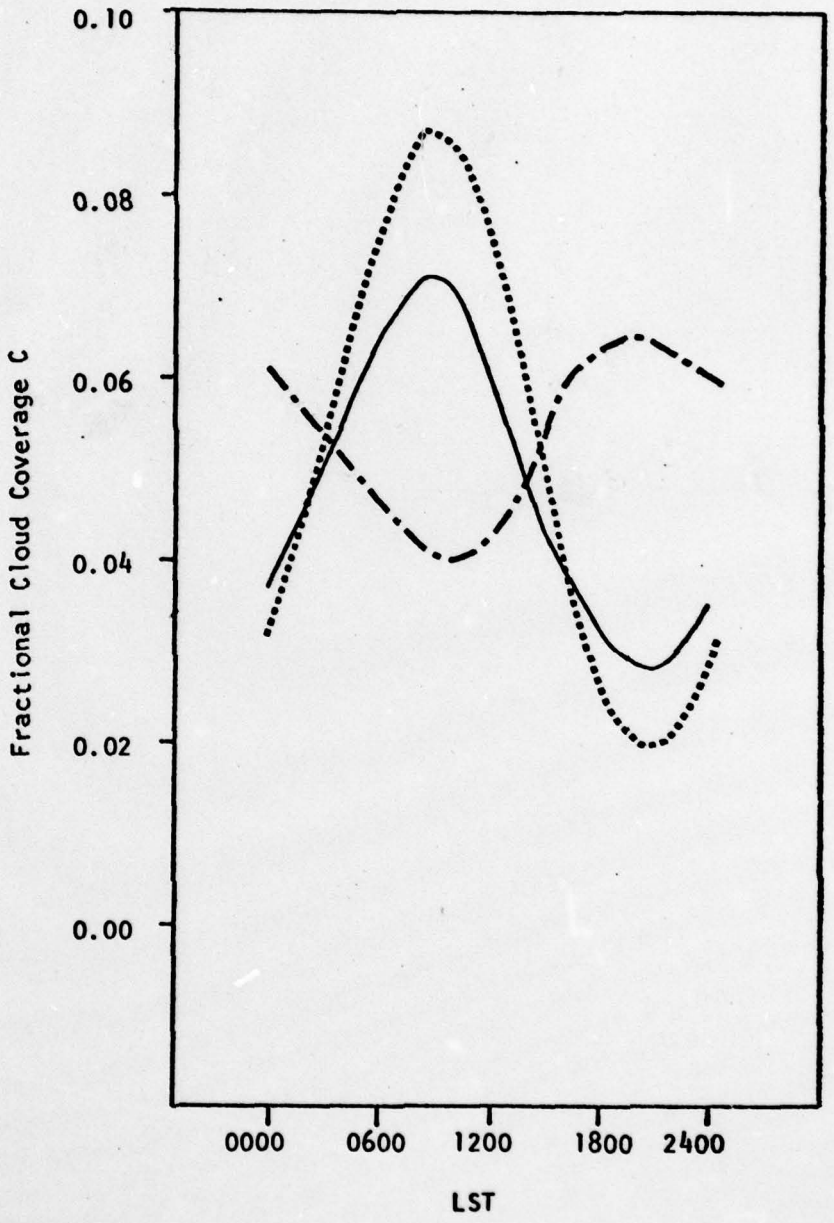

Figure 8. Time series of fractional cloud coverage on day 6 for Experiments I (———), III (- - - -), and IV (— · —).

minimum in the evening. This time lag reflects the fact that individual cumulus clouds do not dissipate immediately when the updrafts in them cease; rather, they are characterized by some finite decay time. Furthermore, the phase exhibited by experiments I and III is in fairly good agreement with that of the diurnal variation in radar echo occurrences over the BOMEX area reported by Hudlow (1970).

As is the case for ω_b^*, C for Experiment III exhibits a smaller diurnal variation than the other experiments and is approximately 180° out of phase to them (see Fig. 8). This again indicates the role of direct radiational heating of the atmosphere in forcing the diurnal fluctuation in cloud activity. Fig. 8 also shows that the diurnal amplitude of C is significantly greater for Experiment III than for Experiment I which again illustrates that the diurnal fluctuation in sea surface temperature tends to suppress the diurnal variation in cloud activity.

Fig. 9 shows time series of precipitation rate P_o. Comparison of Figs. 8 and 9 indicates that the diurnal behavior of the precipitation rate is qualitatively very similar to that of the fractional cloud coverage for all three experiments. This is a reasonable result and is expected in view of the parameterization used for P_o and C (see Equation (98) and (99)).

Fig. 10 shows time series of potential temperature of the atmospheric mixed layer θ_m ($\theta_m = s_m/c_p$). Both Experiments I and III show a minimum in the morning and a maximum in the afternoon. The curve for Experiment I, however, has a slightly larger amplitude than that of

AD-A073 540 SCIENCE APPLICATIONS INC MCLEAN VA OCEAN SCIENCE DIV F/G 4/2
A MODEL OF DIURNAL VARIABILITY OF THE OCEAN-ATMOSPHERE SYSTEM I--ETC(U)
JUL 79 R M CLANCY N00014-78-C-0287
UNCLASSIFIED SAI-79-807-WA NL

2 OF 2
AD A073540

END
DATE FILMED
10-79
DDC

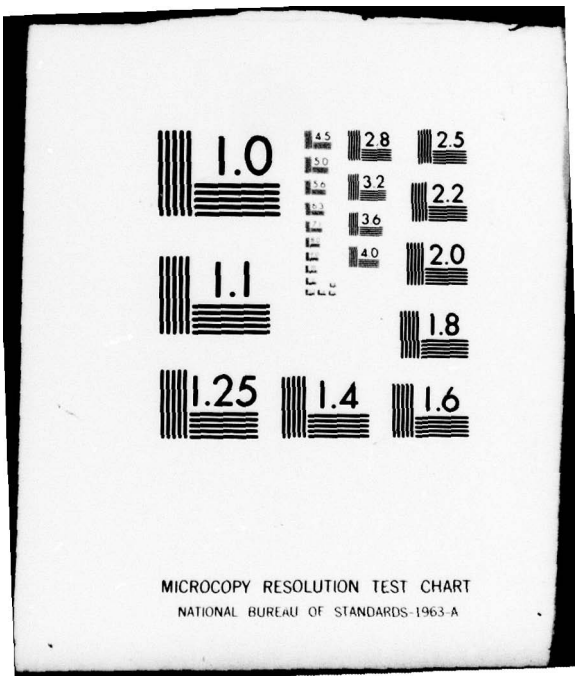
1.0
1.1
1.25
1.4
1.6
1.8
2.0
2.2
2.5
2.8
3.2
3.6
4.0
4.5
5.0
MICROCOPY RESOLUTION TEST CHART
NATIONAL BUREAU OF STANDARDS-1963-A

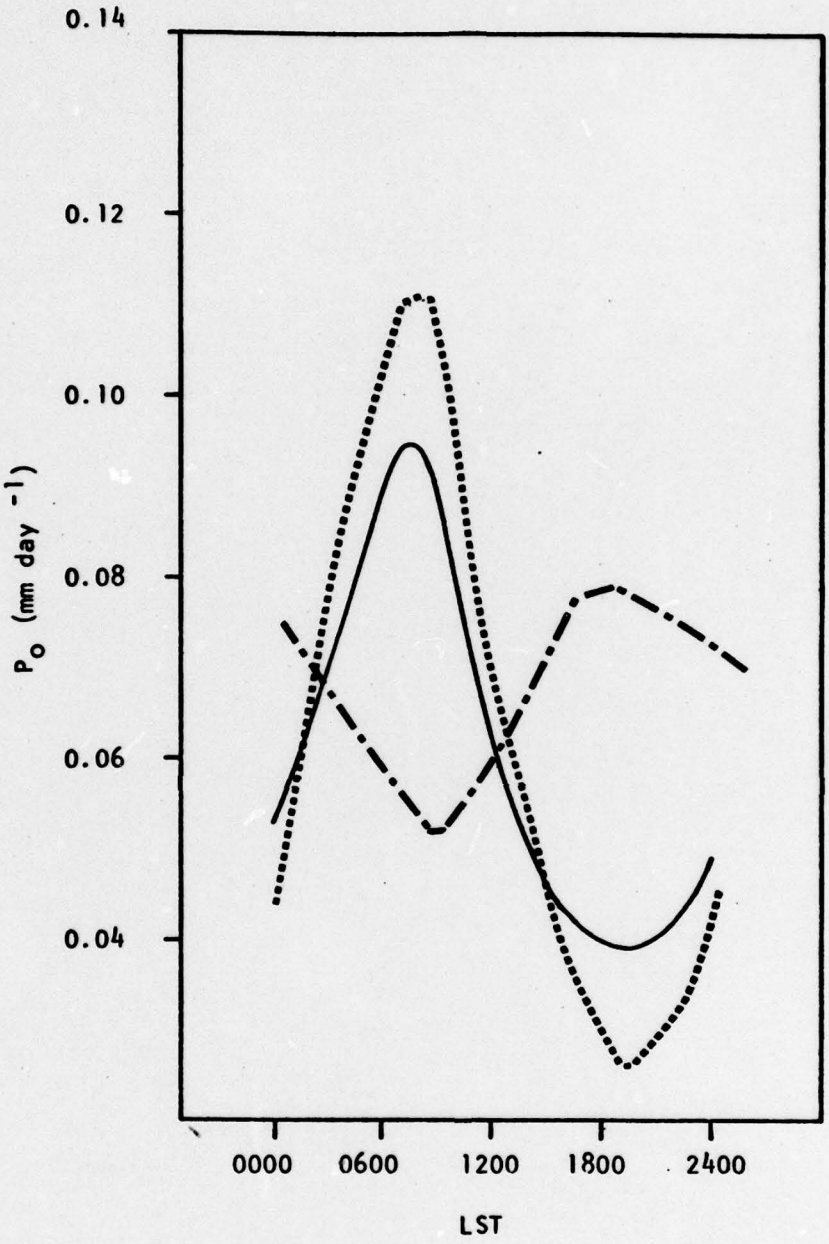

Figure 9. Time series of precipitation rate on day 6 for Experiments I (———), III (-------), and IV (—·——).

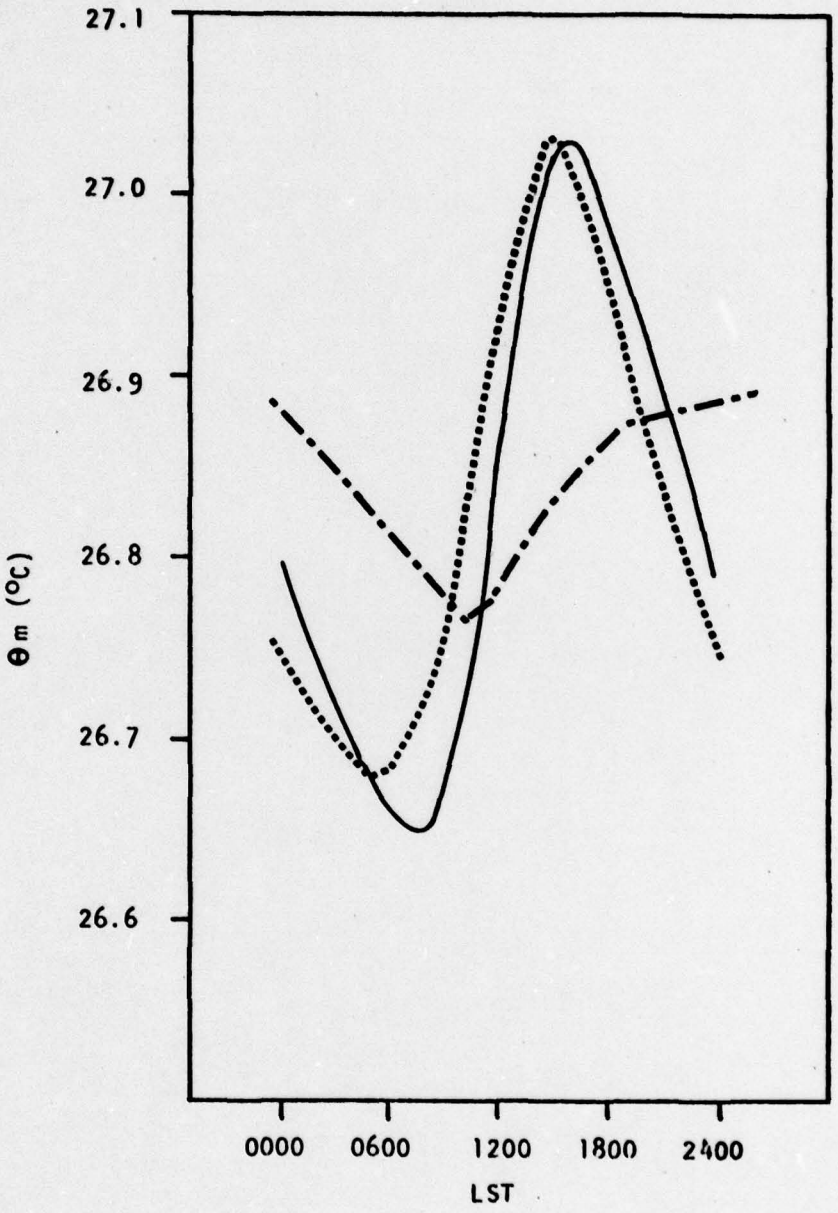

Figure 10. Time series of potential temperature of the atmospheric mixed layer on day 6 for Experiments I (———), and III (------), and IV (—·—·—).

Experiment III and lags it by about 1 hour. Thus, as expected, the diurnally varying sea surface temperature tends to make θ_m slightly cooler in the morning and slightly warmer in the evening. Note that the amplitude and phase of the curve for Experiment I compares favorably with the observations of the diurnal variation in temperature at 11 m height reported by Paulson et al. (1972).

The curve for Experiment IV on Fig. 10 shows a much smaller diurnal variation than those for Experiments I and III and is shifted in phase by about 90° relative to them. Thus we confirm that direct radiational heating of the atmosphere is the mechanism primarily responsible for forcing the diurnal fluctuation in θ_m. This is an expected result.

Fig. 11 shows time series of mixed layer water vapor mixing ratio q_m. Note that the curves for Experiments I and III differ little from one another with both showing minima in the morning and maxima in the afternoon. The amplitude and phase of the curves for Experiments I and III are in good agreement with the observations of the diurnal variation in water vapor mixing ratio at 11 m height reported by Paulson et al.(1972). The curve for Experiment IV, however, shows a much smaller diurnal variation with a maximum at night and a minimum during the day. Thus, the radiational heating of the atmosphere rather than the radiational heating of the ocean (which produces a diurnal variation in q_o) is responsible for forcing the diurnal fluctuation of q_m in Experiments I and III.

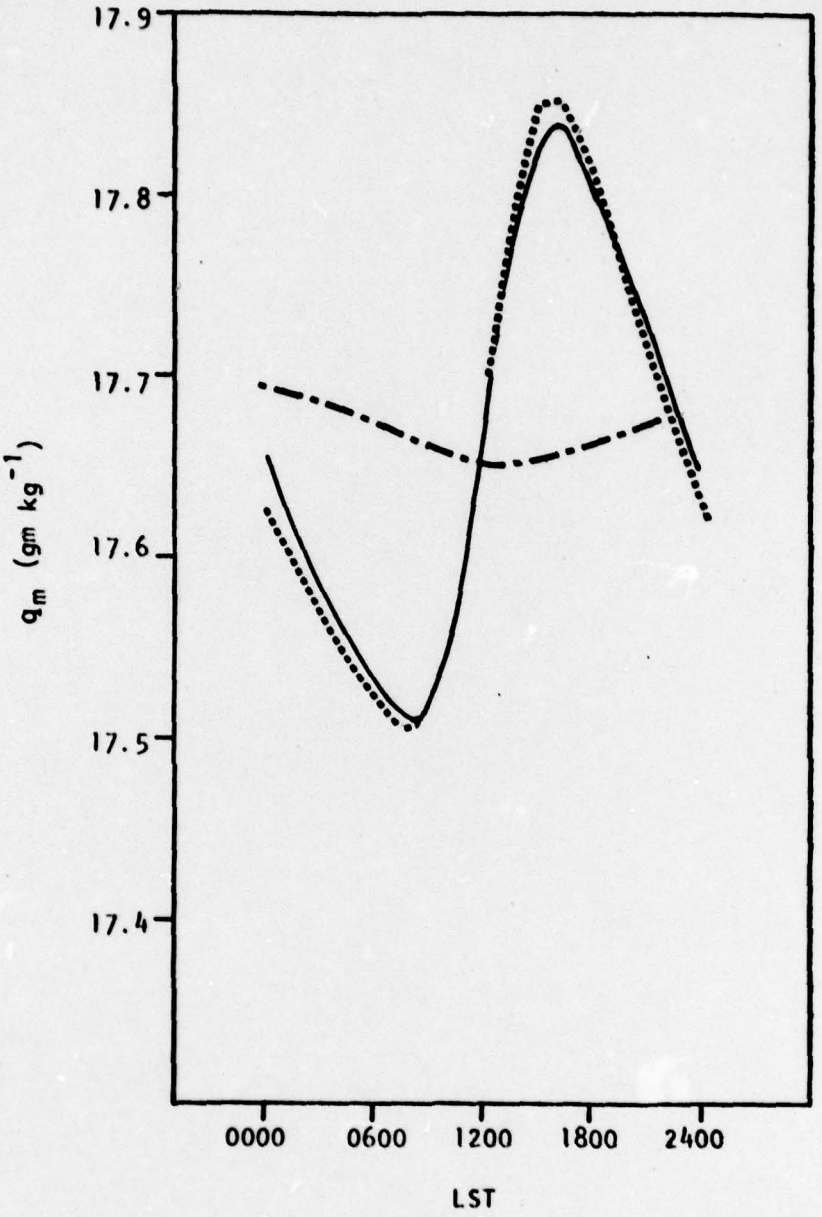

Figure 11. Time series of water vapor mixing ratio of the atmospheric mixed layer on day 6 for Experiments I (———), III (- - - - -), and IV (—·—).

This is an unexpected result since radiational heating, of course, does not appear in the conservation equation for q_m. Consequently, an indirect mechanism linking $\tilde{Q}_R$ to q_m must be present. This mechanism is cumulus convection which is significantly influenced by $\tilde{Q}_R$ (see Fig. 7) and closely linked to the vertical eddy flux of moisture at the top of the atmospheric mixed layer. To illustrate the last point we combine (72) and (77) to write

$$\left(\widetilde{\omega' q}\right)_b = -\Delta q \left(\omega_b^* - \tilde{\omega}_b\right) \tag{100}$$

Thus, since $\Delta q < 0$ and $\omega_b^* < 0$, cumulus convection produces a flux of moisture out of the atmospheric mixed layer at its top ($(\widetilde{w'q'})_b < 0$) which tends to reduce q_m. Recall that for both Experiments I and III, ω_b^* achieves a maximum negative value near midnight and a minimum negative value near midday. Consequently, the atmospheric mixed layer becomes dryer at night as the enhanced cumulus convection pumps moisture up into the cloud layer at a relatively fast rate. During the day when the cumulus convection becomes weaker, moisture is still transported out of the atmospheric mixed layer by the clouds, but at a slower rate. This allows q_m to increase in response to the eddy flux of moisture from the surface. Thus, direct radiational heating of the atmosphere, acting through the mechanism of cumulus convection, controls the diurnal variation of moisture in the atmospheric mixed layer.

Note here that the diurnal fluctuation in cumulus convection also produces a diurnal fluctuation in the eddy flux of dry static energy at the top of the atmospheric mixed layer $(\widetilde{w's'})_b$. However, the impact of this on the diurnal variation of s_m (and hence θ_m) is negligible in Experiments I and III compared to the direct effect of radiational heating in the atmospheric mixed layer (i.e. $(\widetilde{Q}_R)_{ab}$ in Equation (68)).

Fig. 12 shows time series of wind speed at 10 m height U_{10}. For both Experiments I and III, a diurnal variation is clearly present while for Experiment IV the diurnal signal is much less evident. Thus, direct radiational heating of the atmosphere is responsible for forcing the diurnal fluctuation in wind speed in Experiments I and III. The radiational heating of the atmosphere must affect the wind speed through some indirect mechanism and, as was the case for q_m, this indirect mechanism is cumulus convection. The cumulus convection is linked to the eddy flux of momentum at the top of the atmospheric mixed layer in analogous fashion to the moisture flux (see Equation (100)). This eddy momentum flux tends to decrease the wind speed in the atmospheric mixed layer for the choice of large-scale parameters used here. Thus, since the cumulus convection (and, consequently, the eddy momentum flux associated with it) is of greatest intensity at night for Experiments I and III, a minimum in low-level wind speed occurs in these experiments near dawn (see Fig. 12). During the day the cumulus convection weakens and, hence, the low-level wind speed increases, reaching a maximum in the late afternoon.

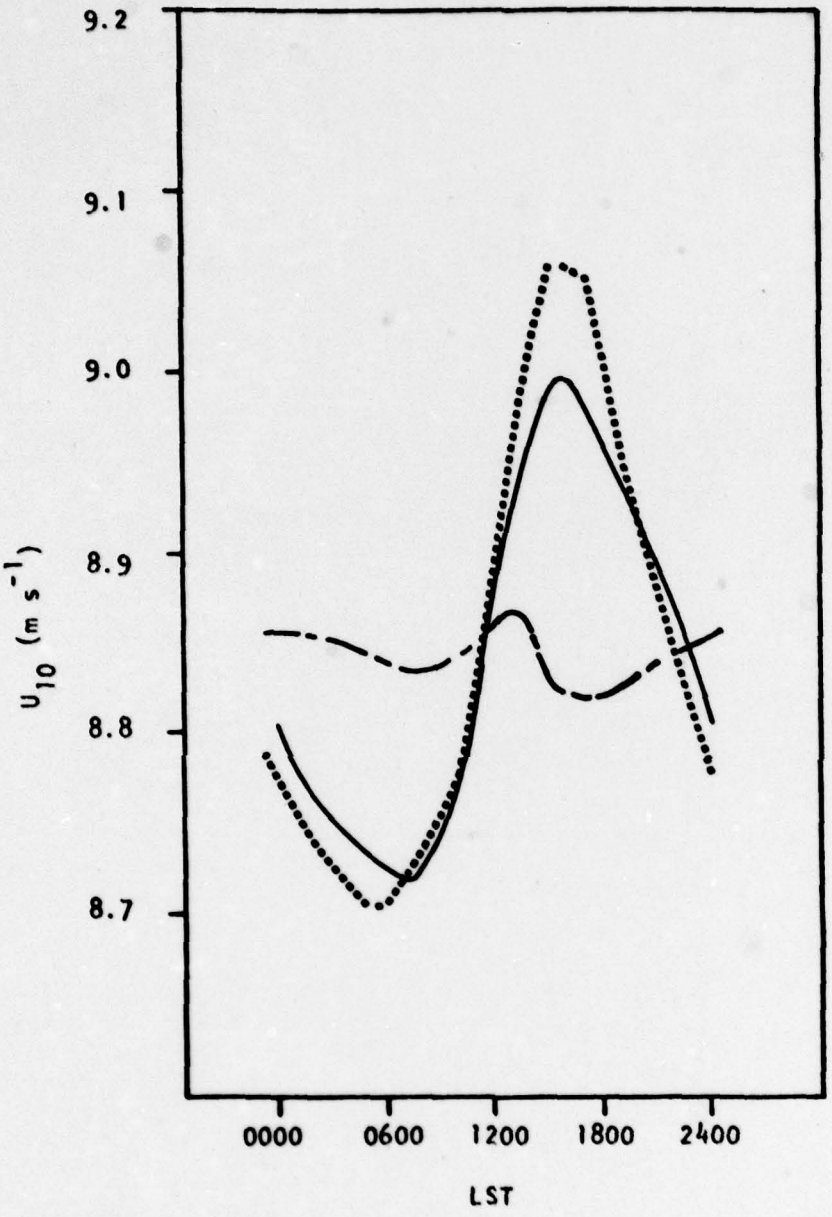

Figure 12. Time series of wind speed at 10 m height on day 6 for Experiments I (———), III (------), and IV (— — —).

So, the diurnal fluctuation in low-level wind speed, as was the case for the diurnal fluctuation in q_m, is controlled primarily by direct radiational heating of the atmosphere through its influence on cumulus convection.

Fig. 13 shows time series of sea surface temperature minus air temperature at 10 m height. This quantity exhibits a broad maximum in the morning and a minimum in the late afternoon which implies that the amplitude of the diurnal fluctuation in low-level air temperature is larger than the amplitude of the diurnal fluctuation in sea surface temperature. This is consistent with several sets of observations made in the tropics including those of Paulson et al. (1972).

Note also from Fig. 13 that the curves for all three experiments differ substantially from one another both in amplitude and phase. This is also the case for the time series of $q_o - q_{10}$ shown in Fig. 14, which appear very similar to the curves of Fig. 13. Thus, direct radiation heating of both the atmosphere and the ocean are found to be important in forcing the diurnal fluctuations in sea-air temperature and moisture differences in Experiment I.

Fig. 15 shows time series of surface sensible heat flux H_o. As is the case for $T_o - T_{10}$, the three curves differ substantially from one another, indicating that direct radiational heating of both the atmosphere and the ocean play an important role in forcing the diurnal fluctuation in H_o. Note also from Figure 15 that H_o for Experiment I achieves a maximum near midday and a minimum near sunset and has a diurnal amplitude of about 2 ly day^{-1}. The phase of this diurnal fluctuation in H_o is

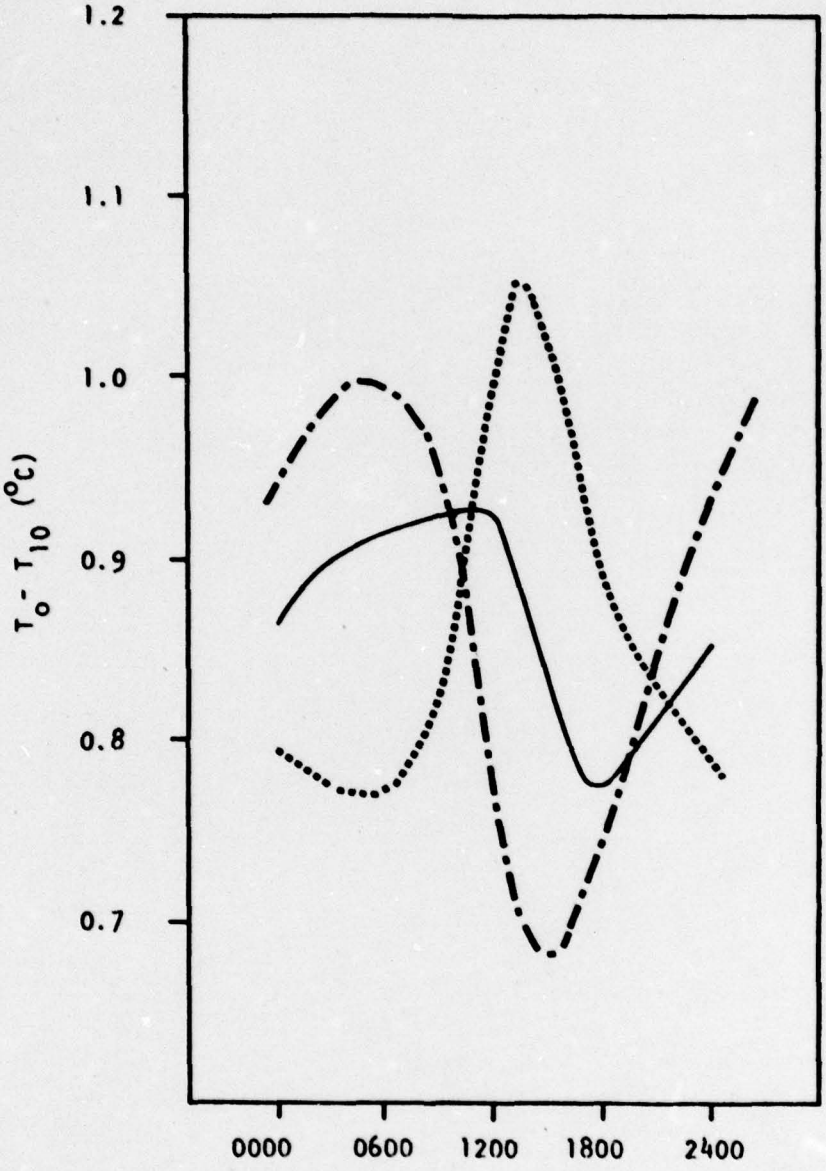

Figure 13. Time series of sea surface temperature minus air temperature at 10 m height on day 6 for Experiments I (———), III (------), and IV (—·—·—).

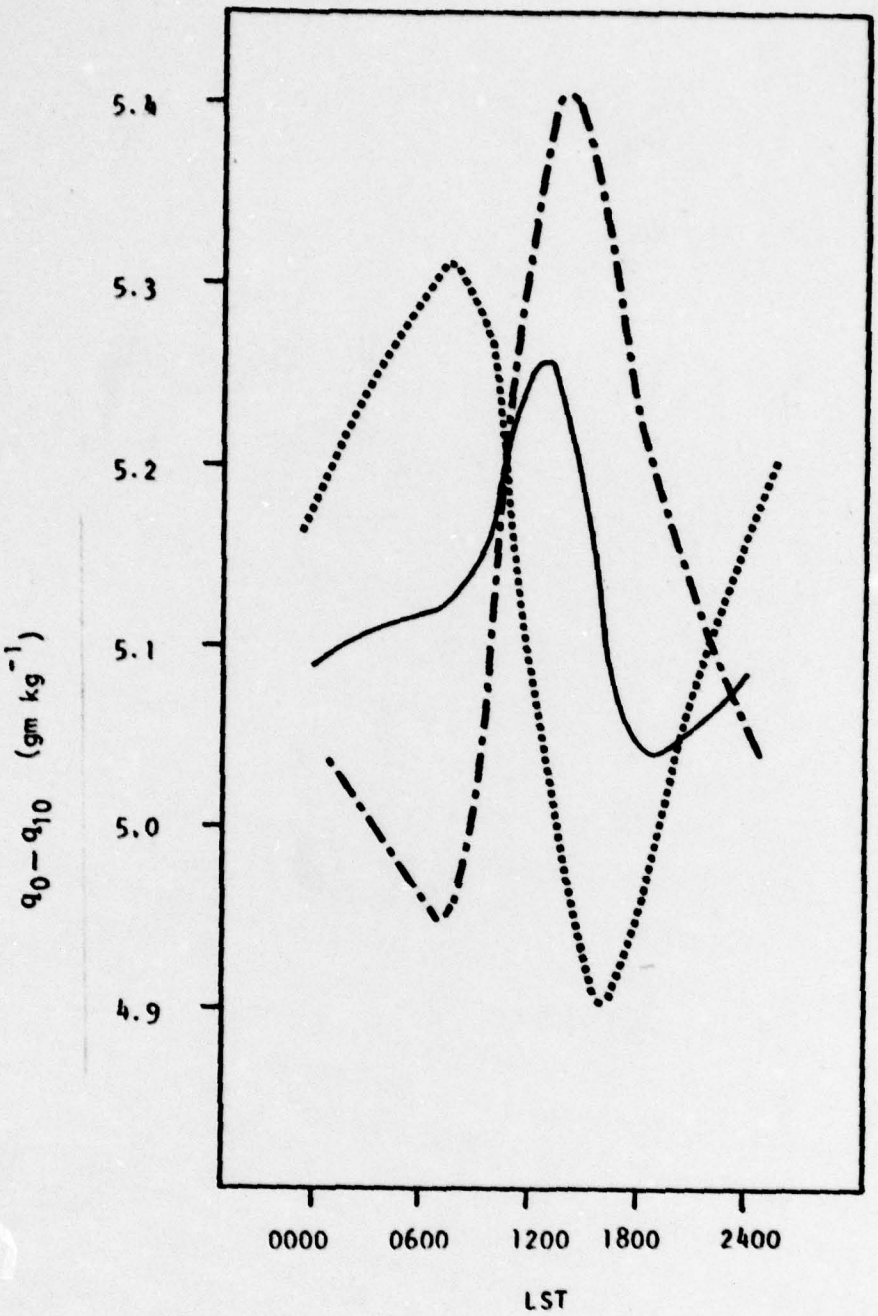

Figure 14. Time series of water vapor mixing ratio at sea surface minus water vapor mixing ratio at 10 m height on day 6 for Experiments I (———), III (- - - - - -), and IV (——·——).

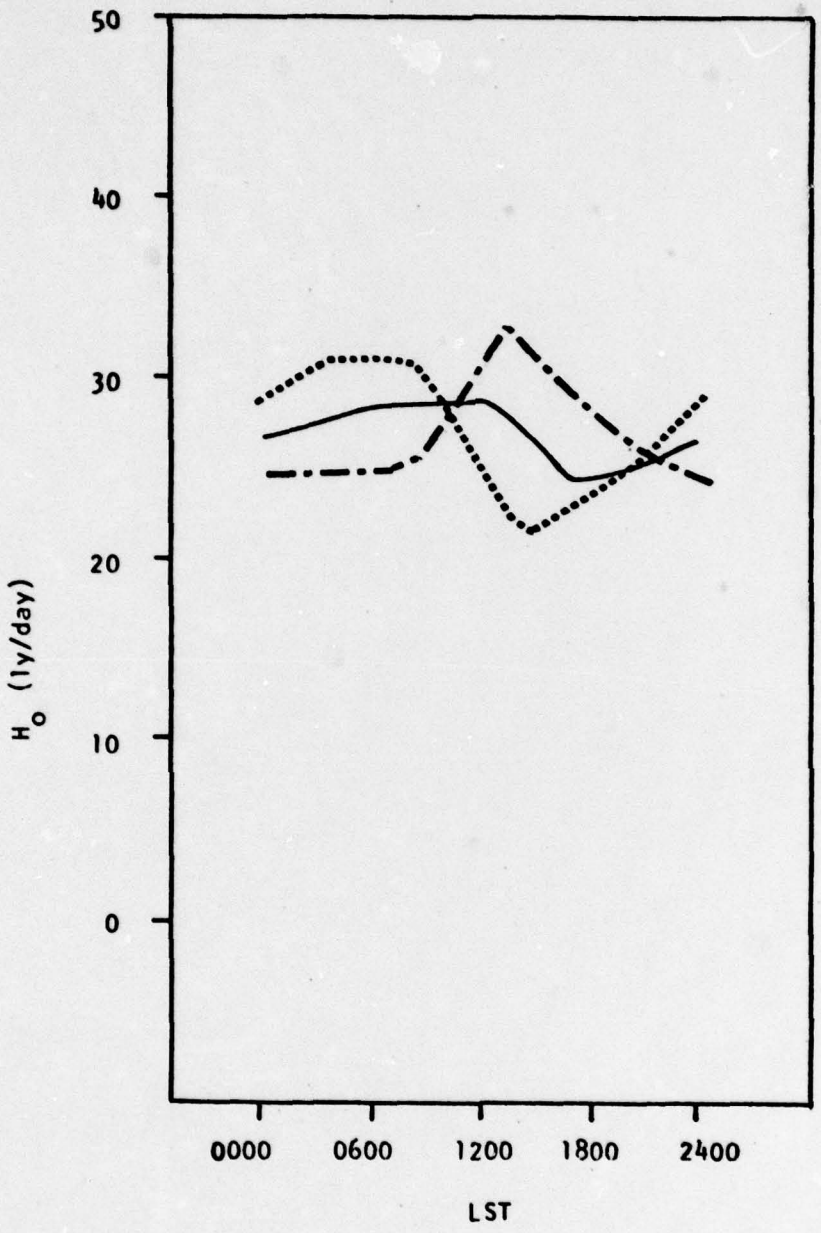

Figure 15. Time series of surface sensible heat flux on day 6 for Experiments I (———), III (·····), and IV (—·—).

consistent with that predicted by Pandolfo and Jacobs (1972) who also modeled BOMEX Phase III with a coupled air-sea model, but the amplitude is only about one half that of the earlier study.

Fig. 16 shows time series of surface latent heat flux L_vQ_o. As is the case for H_o, the three curves differ substantially from one another, thus indicating the importance of direct radiational heating of both the ocean and the atmosphere in forcing the diurnal fluctuation in L_vQ_o. For Experiment I, the surface latent heat flux attains a maximum in the early afternoon and a minimum near sunrise and has a diurnal amplitude of about 9 ly day^{-1}. As is the case for the surface sensible heat flux, the phase of this fluctuation is in approximate agreement with that predicted by Pandolfo and Jacobs (1971) but the amplitude is only about one half.

Note also from Figs. 15 and 16 that the Bowen Ratio (H_o/L_vQ_o) averages about 0.07 for Experiment I. Holland (1972) reports that the observed Bowen Ratio fell within the range 0.07 - 0.14 during the undisturbed period of BOMEX. Thus, our predicted value appears to be too small. The same can be said of the results of Pandolfo and Jacobs (1972) who find a Bowen ratio of 0.05 in their coupled-model integration of the undisturbed period of BOMEX.

Finally, from Figs. 15 and 16 we deduce that the amplitude of the surface sensible plus latent heat flux for Experiment I is approximately 9 ly day^{-1} which is about one half that found by Pandolfo and Jacobs (1972). Delnore (1972), on the other hand, calculated the diurnal

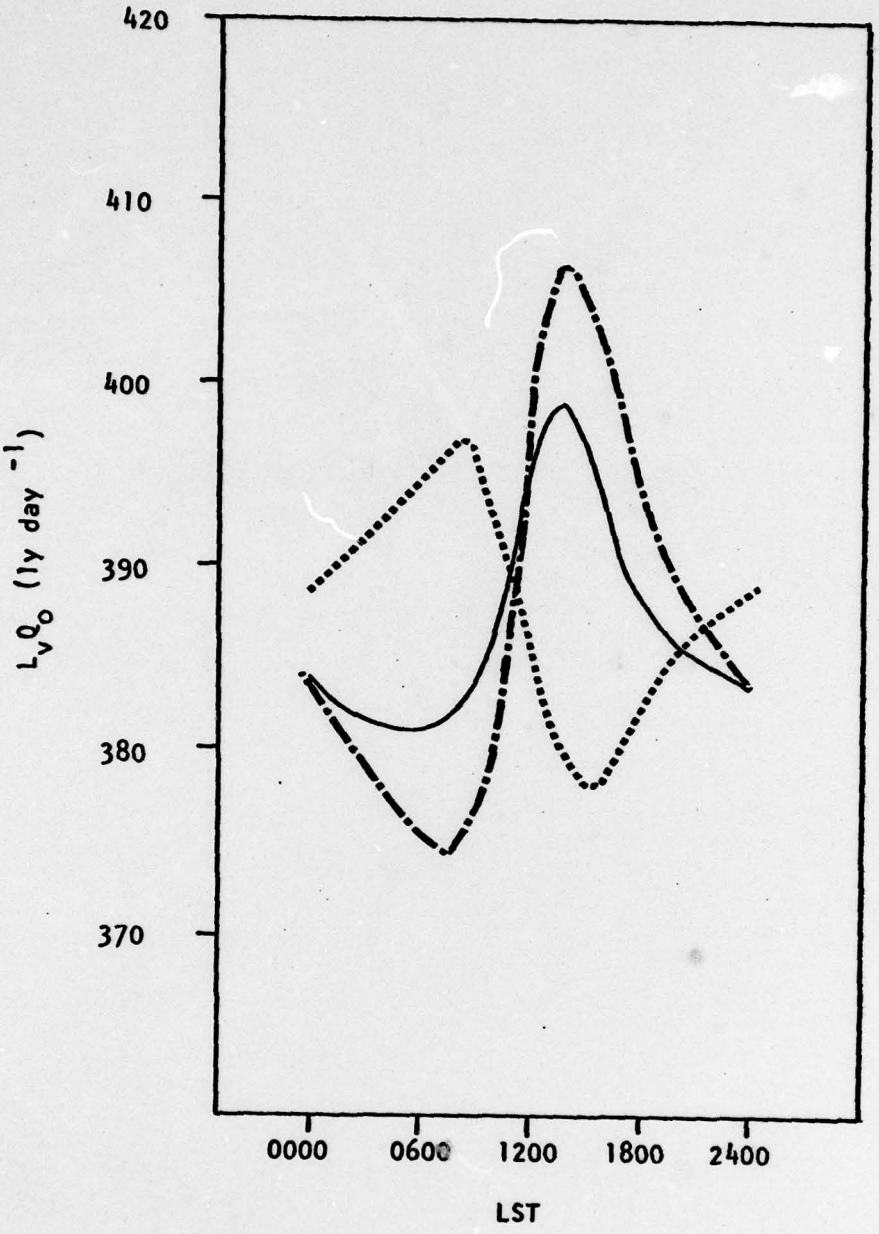

Figure 16. Time series of surface latent heat flux on day 6 for Experiments I (——). III (------), and IV (— — —).

variation of the surface sensible plus latent heat flux from a heat budget for the upper ocean and found the amplitude to be about 400 ly day^{-1} at Discoverer during the period in question. The amplitude calculated by Delnore for this quantity appears unreasonably large since profile measurements by Paulson et al. (1972) in the BOMEX area during May of 1969 did not show these large fluctuations. Rather, Paulson et al. (1972) found fluctuations of $H_o + L_v Q_o$ with amplitudes of about 15 - 20 ly day^{-1}, although they were not purely diurnal. Delnore's (1972) apparent overestimate for the diurnal amplitude of the surface sensible plus latent heat flux may have been partially due to his neglect of solar radiation penetrating below the base of the layer for which the heat budget was calculated and his inexact knowledge of the reflectivity of the sea surface at low sun angles. In addition, as emphasized by Stommel et al. (1969), internal waves on the diurnal thermocline and horizontal inhomogeneities in the upper ocean are quite capable of yielding anomalous surface heat fluxes from this type of budget calculation.

Section 5
SUMMARY AND CONCLUSIONS

We have used coupled air-sea models to investigate diurnal variability of the upper ocean and lower atmosphere in the undisturbed trade wind regime. The oceanic mixed layer is treated with two different models: a diffusive model which uses the closure technique of Mellor and Yamada (1974) to determine the eddy coefficients and a bulk model which uses the entrainment hypothesis and mean-turbulent-field modeling technique of Garwood (1977). A very simple "bulk" model of the lower atmosphere that requires explicit parameterization of the vertical eddy fluxes only at the top and bottom of the atmospheric mixed layer is coupled to both ocean models. The eddy fluxes at the top of the atmospheric mixed layer are parameterized by using some of the ideas from the model of Arakawa and Schubert (1974); the eddy fluxes at the bottom of the atmospheric mixed layer are parameterized using Monin-Obukhov similarity theory. A simple parameterization of rainfall rate closes the model atmosphere.

Time-independent values for the horizontal advection of all quantities, the vertical component of the fluid motion, the geostrophic component of the fluid motion, and the lapse rates of dry static energy and water vapor mixing ratio in the trade inversion are derived from observations during the undisturbed period of BOMEX Phase III (21 - 26 June 1969) and imposed as large-scale forcing

functions. In addition, the coupled-model is forced temporally with a prescribed diurnally varying radiational heating profile which is also based on the BOMEX data.

The model atmosphere predicts the observed time-averaged low-level temperature profile quite well. The predicted time-averaged water vapor mixing ratio profile also compares quite favorably with the observations except in the upper two thirds of the atmospheric mixed layer. This discrepancy occurs because the observations do not show a high degree of vertical uniformity for water vapor mixing ratio in the atmospheric mixed layer, while complete uniformity of the quantitiy is assumed there in the model.

The time-averaged surface sensible plus latent heat flux predicted by the model is close to the average of several values for this quantity calculated by various authors from the BOMEX data. The model-predicted Bowen Ratio, however, appears to be too small.

Both the diffusive and bulk models of the oceanic mixed layer give good predictions of the upper ocean thermal structure near sunrise. This can be attributed to the fact that the net surface heat flux changes slowly at night, which allows the upper ocean to approach an equilibrium state with the surface forcing. During the day, however, when the net surface heat flux changes rapidly with time because of the solar radiative flux, the diffusive model performs noticeably better than the bulk model. This is partly due to a fundamental difference between diffusive and bulk models: a diffusive model mixes heat supplied near the surface

downward on some finite time scale while a bulk model assumes that heat supplied near the surface is mixed instantaneously throughout the mixed layer. In addition, the bulk model used here predicts that all turbulence ceases below a few meters depth near the time of maximum solar heating. The diffusive model, on the other hand, predicts that turbulent mixing always extends down to a depth of at least 15 m for the cases considered, which seems to be a more realistic result in view of the observed temperature profiles.

Diurnal variations of cumulus cloud activity, low level temperature, moisture, and wind speed in the coupled model are found to be forced primarily by direct radiational heating of the atmosphere rather than by direct radiational heating of the ocean and its associated diurnal fluctuation in sea surface temperature. The direct radiational heating of the atmosphere forces the diurnal fluctuation in cloud activity through its effect on the "cloud layer forcing term" (see Arakawa and Schubert, 1974). This, in turn, produces a diurnal variation in low-level moisture and wind speed through cloud-related vertical eddy fluxes of moisture and momentum at the top of the atmospheric mixed layer.

The diurnal fluctuation of the surface sensible plus latent heat flux is controlled by both direct radiational heating of the atmosphere and direct radiational heating of the ocean. However, the amplitude of this fluctuation is about two orders of magnitude smaller than the amplitude of the surface solar flux which is primarily responsible for driving the diurnal sea surface temperature fluctuation.

Although the sea surface temperature fluctuation alters the surface solar flux through its influence on cloud cover, this alteration is extremely small. Therefore, the feedback loop between the ocean and the atmosphere is exceedingly weak at the diurnal time scale.

The present study could be extended in several ways. First, an attempt could be made to parameterize the evaporation of spray just above the sea surface which may be an important process in regions where the low-level wind speed is strong (Ling and Kao (1976), Wang and Street (1978)). Neglect of this process may be part of the reason why the Bowen Ratio predicted by the coupled-model is too small.

In addition, if the vertical eddy fluxes of dry static energy, water vapor mixing ratio, and liquid water mixing ratio at the base of the trade inversion could be parameterized along with the vertical distribution of the raindrop generation rate, the lapse rates of temperature and humidity in the trade inversion could be predicted rather than imposed quantities. Although this would make the model atmosphere much more empirical, it would also make it more general. In this case it could provide an economical yet detailed parameterization of the planetary boundary layer over the tropical ocean in an atmospheric general circulation model.

APPENDIX

LIST OF SYMBOLS

$A(\lambda)$	Cloud work function for type λ clouds
A_H, A_M	Stability functions for eddy coefficients in oceanic mixed layer
a_1	Proportionality constant in definition of transport time scale for oceanic mixed layer
B_o	Surface flux of infrared radiation
b_*	Stefan-Boltzmann Constant
b	Buoyancy
C	Cloud cover
c	Specific heat for seawater
c_p	Specific heat at constant pressure for air
D	Damping coefficient for inertial oscillations
E	Turbulent kinetic energy in oceanic mixed layer
$F(\lambda)$	Large-scale forcing for type λ clouds
F_A	Characteristic large-scale forcing for cumulus cloud ensemble
F_M	Contribution of mixed-layer forcing to F_A
F_C	Contribution of cloud-layer forcing to F_A

F_o	Flux of solar radiation penetrating sea surface
F_i	Flux of solar radiation penetrating sea surface in the absence of clouds
f	Coriolis parameter
g	Acceleration of gravity
H_o	Surface sensible heat flux
h	Depth of oceanic mixed layer
I_o	Surface flux of the penetrating component of solar radiation
$\hat{i}, \hat{j}, \hat{k}$	Unit vectors in the x, y, z directions
K_H, K_S, K_M	Vertical eddy diffusion coefficients for heat, salinity, and momentum in ocean
$K(\lambda,\lambda')$	Kernel from Arakawa-Schubert cumulus parameterization theory
K_A	Characteristic kernel for cumulus cloud ensemble
k_1, k_2, k_3	Empirical proportionality constants for model atmosphere
L	Monin-Obukhov length
L_v	Latent heat of evaporation
ℓ	Turbulence length scale for oceanic mixed layer
LST	Local Standard Time

$m_b(\lambda)$	Cloud base mass flux for type clouds
m_4	Critical constant parameter governing entrainment in bulk model of oceanic mixed layer
M	Total number of active updrafts in cumulus ensemble
$n_i(i=1,8)$	Empirical constants in diffusive model of the oceanic mixed layer
N	Total number of clouds in cumulus ensemble
p, p_a, p_b	Pressure, pressure at top of surface layer, top of mixed layer
p_b^-, p_L, p_c	Pressure at top of transition layer, lifting condensation level, base of trade inversion
p_d	Pressure at top of trade inversion
P_o	Precipitation rate
q	Water vapor mixing ratio
q_m, q_{10}	Water vapor mixing ratio of atmospheric mixed layer, at 10 m height
Q_o	Surface evaporation rate
Q_R	Net radiational heating rate
Q_C	Rate of condensation minus evaporation per unit mass of air
$\tilde{q}_d$	Water vapor mixing ration at model top
R	Gas constant for dry air

R_f	Flux Richardson number in oceanic mixed layer
s	Dry static energy
s_m	Dry static energy of atmospheric mixed layer
S	Salinity
S_m	Salinity of oceanic mixed layer
S_w	Reference salinity
$\tilde{s}_d$	Dry static energy at model top
T	Temperature
T_o	Temperature at sea surface
T_{10}	Temperature at 10 m height
T_a, T_w	Reference temperature for air, water
T_m	Temperature of oceanic mixed layer
t	Time
u	x-directed component of current velocity vector, wind velocity vector
U, U_o, U_{10}	Wind speed, wind speed at sea surface, wind speed at 10 m height
u_*	Surface friction velocity in air
U_m	Mixed-layer wind speed

v	y-directed component of current velocity, wind velocity
$\underline{v}_m$	Horizontal current velocity vector, wind velocity vector
$\underline{v}$	Mixed layer horizontal current velocity vector, wind velocity vector
$\underline{v}_g$	Geostrophic current velocity vector, wind velocity vector
$(\underline{v}_g)_o$	Geostrophic wind velocity vector at sea surface
w	Vertical component of current velocity
w_e	Entrainment velocity
W	Liquid water mixing ratio
W_i	Liquid water mixing ratio of i th cloud
W_A	Characteristic value of liquid water mixing ratio for typical cloud in the ensemble
x, y, z	Cartessian coordinates; x positive eastward, y positive northward, z positive upward, from the sea surface
z_o	Surface roughness length
α	Thermal expansion coefficient for seawater

β	Saline expansion coefficient for seawater
γ	Extinction coefficient for radiation in ocean
ε	Infrared emissivity of sea surface
κ	Von Karmen's constant
θ, θ_m	Potential temperature, potential temperature of atmospheric mixed layer
ϕ_θ, ϕ_q, ϕ_m	Non-dimensional vertical derivative of temperature, water vapor mixing ratio, wind speed in surface layer
ρ	Density
ρ_w, ρ_a	Reference density for water, air
σ	Fraction of model domain covered by active cloud updrafts
λ	Entrainment rate
σ_i	Fraction of model domain covered by i th cloud updraft
τ_e	Turbulent transport time scale in oceanic mixed layer
$\underset{\sim}{\tau}_o$	Suface wind stress vector
ω	Vertical p-velocity

ω^*	Cloud-produced vertical p-velocity
ω_i^*	Vertical p-velocity in i th cloud updraft
ΔT, ΔS	Change in temperature, salinity across entrainment zone at base of oceanic mixed layer
Δs, Δq	Change in dry static energy, water vapor mixing ratio across transition layer at top of atmospheric mixed layer
$\Delta \underline{v}$	Change in horizontal velocity vector across either entrainment zone or transition layer
$\left(\frac{\partial \tilde{s}}{\partial p}\right)_I$, $\left(\frac{\partial \tilde{q}}{\partial p}\right)_I$	Lapse rate of dry static energy, water vapor mixing ration in trade inversion

REFERENCES

Albrecht, B.A., 1977. A time-dependent model of the trade-wind boundary layer. Atmospheric Science Paper No. 267, Colorado State University, Fort Collins, Colorado, 174 pp.

Arakawa, A., and W. H. Schubert, 1974. Interaction of a cumulus ensemble with the large-scale environment, Part I. J. Atmos. Sci., 31, 674-701.

Augstein, E., H. Schmidt, and F. Ostapoff, 1974. The vertical structure of the atmospheric planetary boundary layer in undisturbed trade winds over the Atlantic Ocean. Boundary Layer Met., 6, 129-150.

Bates, J. R. 1972. Tropical disturbances and the general circulation. Quart. J. Roy. Met. Soc., 98, 1-16.

Betts, A. K., 1973. Non-precipitating cumulus convection and its parameterization. Quart. J. Roy. Met. Soc., 99, 178-196.

_____, 1975. Parametric interpretation of trade-wind cumulus budget studies. J. Atmos. Sci., 32, 1934-1945.

_____, 1976. Modeling subcloud layer structure and interaction with a shallow cumulus layer. J. Atmos. Sci., 33, 2363 - 2382.

Busch, N. E., 1977. Fluxes in the surface boundary layer over the sea. Chapter 6, Modelling and Prediction of the Upper Layers of the Ocean, Pergamon Press, New York

Businger, J. A., 1975. Interactions of sea and atmosphere. Rev. Geophys. and Space Phys., 13, 720-726.

Clarke, R. H., 1970. Recommended methods for the treatment of the boundary layer in numerical prediction models. Mon. Wea. Rev., 97, 77-85.

Deardorff, J. W., 1978. Observed characteristics of the outer layer. Chapter 5, The Planetary Boundary Layer, American Meteorological Society, Boston.

Delnore, V. E., 1972. Diurnal variation of temperature and energy budget for the oceanic mixed layer during BOMEX. J. Phy. Ocean., 2, 239-247.

Denman, K. L., 1973. A time-dependent model of the upper ocean. J. Phys. Ocean., 3, 173-184.

Ekman, V. W., 1905. on the influence of the earth's rotation on ocean currents. Av. Kiv. Mat. Ashon. Fysik., 2, 1-53.

Elsberry, R. L., T. S. Fraim, and R. N. Trapnell, 1976. A mixed layer model of the oceanic thermal response to hurricanes. J. Geophys. Res., 81, 1153-1162.

Esbensen, S., 1978. Bulk thermodynamic effects and properties of small tropical cumuli. J. Atmos. Sci., 35, 826-837.

Garstang, M., and A. K. Betts, 1974. A review of the tropical boundary layer and cumulus convection: Structure, parameterization and modeling. Bull. Amer. Meteor. Soc., 55, 1195-1205.

Garwood, R. W., 1977. An oceanic mixed layer model capable of simulating cyclic states. J. Phys. Ocean., 7, 455-468.

Grassl, H., 1976. The dependence of the measured cool skin of the ocean on wind stress and total heat flux. Bound. Lay. Met., 10, 465-474.

Gray, W. M., and R. W. Jacobson, 1977. Diurnal variation of deep cumulus convection. Mon. Wea. Rev., 105, 1171-1188.

Hann, J., 1901. Lehrbuch der Meteorologie, 1 st ed. Chr. Herm Tachnitz, Leipzig, 338-346.

Hogstrom, U., 1974. A field study of the turbulent fluxes of heat, water vapor and momentum at a "typical" agricultural site. Quart. J. Roy. Met. Soc., 100, 624-639.

Holland, J. Z., and E. M. Rasmusson, 1973. Measurements of the atmospheric mass, energy, and momentum budgets over a 500-kilometer square of tropical ocean. Mon Wea. Rev., 101, 44-55.

Hudlow, M.D., 1970. Weather radar investigations on the BOMEX. Research and Development Report ECOM-3320, U.S. Army Electronics Command, Fort Monmouth, N. J., 106 pp.

Jacobs, C. A., 1978. Numerical simulations of the natural variability in water temperature during BOMEX using alternative forms of the vertical eddy exchange coefficients. J. Phy. Ocean., 8, 119-141.

Jacobson, R. W., Jr., 1976. Diurnal variation of oceanic deep cumulus convection, Part II: Observational evidence Pap. No. 243, Dept. Atmos. Sci., Colorado State University, 106 pp.

Kolmogoroff, A. N., 1942. The equations of turbulent motion in an incompressible fluid. Izv. Akad. Nauk SSR, Ser. Fig., 6, No. 1, 2, 56-58.

Kraus, E. B., 1963. The diurnal precipitation change over the sea. J. Atmos. Sci., 20, 551-556.

_____, and J. S. Turner, 1967. A one-dimensional model of the seasonal thermocline: II. The general theory and its consequences. Tellus, 19, 98-106.

_____, 1972. Atmosphere-Ocean Interaction. Clarendon Press, Oxford.

_____, 1977. Ocean surface drift velocities. J. Phy. Ocean., 7, 606-609.

Kuettner, J. P., and J. Holland, 1969. The BOMEX Project. Bull. Amer. Meteor. Soc., 50, 394-402.

Lavoie, R.L., 1963. Some aspects of the meteorology of the tropical Pacific viewed from an atoll. Rep. No. 27, Institute of Geophysics, University of Hawaii, 76 pp.

Ling, S. C., and T. W. Kao, 1976. Parameterization of the moisture and heat transfer process over the ocean under white-cap sea states. J. Phy. Ocean., 6, 306-315.

Mamayev, O. I., 1958. The influence of stratification on the vertical turbulent mixing in the sea. Bull. Acad. Sci. USSR Geophys. Ser., 7, 494-497.

Martin, P. J., 1976. A comparison of three diffusion models of the upper mixed layer of the ocean. NRL Memorandum Report 3399, Naval Research Laboratory, Washington, D.C.

_____, and J. D. Thompson, 1978. Formulation and testing of a layer-compatible upper ocean mixed-layer model. Submitted to J. Phy. Ocean.

Mellor, G. L., and T. Yamada, 1974. A hierarchy of turbulence closure models for planetary boundary layers. J. Atmos. Sci., 31, 1791-1806.

_____, and P. A. Durbin, 1975. The structure and dynamics of the ocean surface mixed layer. J. Phy. Ocean., 5, 718-728.

Monin, A. S. and A. M. Obukhov, 1954. Basic laws of turbulent mixing in the ground layer of the atmosphere, Akad. Nauk. SSSR, Geofiz. Inst. Trudy, 151, 163-187.

Munk, W. and E. R. Anderson, 1948. Notes on a theory of the thermocline. J. Mar. Res., 7, 276-295.

Niiler, P. and E. B. Kraus, 1977. One-dimensional models of the upper ocean. Chapter 10, Modelling and Prediction of the Upper Layers of the Ocean, Pergamon Press, New York.

Niiler, P. 1975. Deepening of the wind-mixed layer. J. Mar. Res., 33, 405-422.

Nitta, T., 1975. Observational determination of cloud mass flux distributions. J. Atmos. Sci., 32, 73-91.

_____, and S. Esbensen, 1974. heat and moisture budget analyses using BOMEX data. Mon. Wea. Rev., 102, 17-28.

_____, and S. Esbensen, 1974. Diurnal variations in the western Atlantic trades during the BOMEX. J. Meteor. Soc. Japan, 52, 254-257.

Ogura, Y., 1972. Clouds and convection. Parameterization of Subgrid-scale Processes, GARP Publ. Ser., No. 8, 20-39.

_____, and H-R Cho, 1974. On the interaction between the subcloud and cloud layers in tropical regions. J. Atmos. Sci., 31, 1850- 1859.

Ostapoff, F., and S. Worthem, 1974. The intradiurnal temperature variation in the upper ocean layer. J. Phy. Ocean., 601-612.

Pandolfo, J. P., 1969. Motions with inertial and diurnal period in a numerical model of the navifacial boundary layer. J. Mar. Res., 27, 301-317.

_____, 1971. numerical experiments with alternative boundary layer formulations using BOMEX data. Boundary-Layer Meteorol., 1, 277-289.

_____, and C. A. Jacobs, 1972. Numerical simulations of the tropical air-sea planetary boundary layer. Bound.-Layer Meteor., 3, 15-46.

Paulson, C. A., Leavitt, E., and R. G. Fleagle, 1972. Air-sea transfer of momentum, heat and water determined by profile measurements during BOMEX. J. Phy. Ocean., 2, 487-497.

Paulson, C. A., 1970. The mathematical representation of wind speed and temperature profiles in the unstable atmospheric surface layer. J. Appl. Meteor., 9, 857-861.

Pennell, W. T. and M. A. Lemone, 1974. An experimental study of turbulence structure in the fair-weather trade wind boundary layer. J. Atmos. Sci., 31, 1308-1323.

Pollard, R. T. and R. C. Millard, Jr., 1970. Comparison between observed and simulated wind-generated inertial oscillations. Deep-Sea Res., 17, 813-821.

Roll, H. U., 1965. Physics of the Marine Atmosphere, Academic Press, 426 pp.

Rotta, J. C., 1951. Statistiche theorie michthomogener turbulenz. Z. Phys., 129, 547-572.

Schubert, W. H., 1976. Experiments with Lilly's cloud-topped mixed layer model. J. Atmos. Sci., 33, 436-446.

Shonting, D.H., 1964. Observations of short term heating of the surface layers of the ocean TM No. 308, U.S. Naval Underwater Ordnance Station, Newport, Rhode Island, 22 pp.

Soong, S-T. and Y. Ogura, 1976. A determination of the trade-wind cumuli population using BOMEX data and an axisymmetric cloud model. J. Atmos. Sci., 33, 992-1007.

Stommel, H., K. Saunders, W. Simmons, and J. Cooper, 1969. Observations of the diurnal thermocline. Deep-Sea Res., 16, 269-284.

Urick, R. J., 1975. Principles of Underwater Sound. McGraw-Hill, Inc., 384 pp.

Vager, B. G., and S. S. Zilitinkevich, 1968. A theoretical model of the diurnal variations of the meteorological fields. Meteorol. i. Gidrol, 7.

Wang, C. S. and R. L. Street, 1978. Transfers across an an air-water interface at high wind speeds: The effect of spray. J. Geophys. Res., 83, 2959-2969.

Wyrtki, K., 1965. The average annual heat balance of the North Pacific Ocean and its relation to ocean circulation. J. Geophys. Res., 70, 4547-4559.

DISTRIBUTION LIST

NORDA, NSTL Station, MS 39529
S.A. Piacsek, Code 322 (3 Copies)
RM Clancy, Code 322 (12 Copies)
Library

NAVOCEANO
NSTL Station, MS 39529
Library
J. Peloquin
M. Shanks

Fleet Numerical Weather Central
Monterey, CA 93940
Commanding Officer
Library
Leo Clark
Jack Kaitala

Environmental Prediction
Research Facility
Monterey, CA 93940
Commanding Officer
Library
T. Rosmond

Naval Postgraduate School
Monterey, CA 93940
Library
R. Haney
R. W. Garwood
R. Elsberry

NRL Code 2627 (6 Copies)
Washington, D.C. 20375

ONR Code 102IP (6 Copies)
800 N. Quincy Street
Arlington, VA 22217

DDC (12 Copies)
Bldg 5, Cameron Station
Alexandria, VA 22314

ONR
495 Summer St.
Boston, MA 02210

Dr. Richard Lau (2 Copies)
ONR
1030 East Green St.
Pasadena, CA 91106

Contracting Officer
ONR Code 613C: JMD
800 N. Quincy Street
Arlington, VA 22217

G. O. Roberts (4 Copies)
SAI
McLean, VA 22102

Total of 62 copies

MEMORANDUM

TO: Distribution List DATE: 27 August 1979

FROM: Dr. Glyn O. Roberts
Ocean Science Division

REFERENCE: CONTRACT N00014-78-C-0287

- -

As authorized by Dr. Steve A. Piacsek, the scientific officer, SAI is pleased to enclose herewith its final report on the referenced contract. The report is in two parts:

> "The Effect of Inaccuracies in Meteorological Parameters on One Dimensional Forecasts of Upper Ocean Thermal Structure", Report SAI-79-880-WA; and
>
> "A Model of Diurnal Variability of the Ocean Atmosphere System in the Undisturbed Trade Wind Regime", Report SAI-79-807-WA.

Our distribution list includes that required by the contract.

Enclosures